Generation of mesoscale eddies in the lee of the Hawaiian Islands

Y. Jia,[1] P. H. R. Calil,[2] E. P. Chassignet,[3] E. J. Metzger,[4] J. T. Potemra,[1] K. J. Richards,[1] and A. J. Wallcraft[4]

[1] The ocean west of the main Hawaiian Islands is characterized by enhanced eddy kinetic energy arising from the abundance of locally generated mesoscale eddies, most frequently in the area west of the island of Hawaii. Two mechanisms of eddy generation in the wake of an island are examined with numerical model experiments. The first, eddy generation and shedding by an oceanic flow around an oceanic barrier, requires the existence of strong westward flows to the north and south of the island of Hawaii. Model solutions show such westward flows and generation of eddies by these flows although the intensity of the eddies and the generation frequency are much lower than that derived from altimetry. As a result, these eddies contribute an insignificant amount of eddy kinetic energy in the region. The second, eddy generation and shedding by an atmospheric flow around an atmospheric barrier, is based on oceanic upwelling and downwelling induced by surface wind shear, effectively introducing sinks and sources to the ocean interior. Previous idealized modeling studies have shown that oceanic eddies can be generated by sufficiently strong forcing (source or sink), providing an explanation why eddy occurrences in the lee of the island of Hawaii coincide with periods of strong trade winds. Eddy generation characteristics in the model experiments are consistent with this mechanism in terms of time of occurrence, strength and the resulting eddy kinetic energy. Major discrepancies are in eddy propagation and therefore eddy distribution in the regional domain due to the complex nature of eddy-eddy interactions.

Citation: Jia, Y., P. H. R. Calil, E. P. Chassignet, E. J. Metzger, J. T. Potemra, K. J. Richards, and A. J. Wallcraft (2011), Generation of mesoscale eddies in the lee of the Hawaiian Islands, *J. Geophys. Res.*, *116*, C11009, doi:10.1029/2011JC007305.

1. Introduction

[2] Mesoscale eddies abound west of the main Hawaiian Islands, resulting in locally enhanced eddy kinetic energy [*Kobashi and Kawamura*, 2001; *Calil et al.*, 2008]. While some eddies propagate into the region from the east, the majority are generated locally. In particular, strong cyclonic and anticyclonic eddies have been observed to emerge west (lee side) of the island of Hawaii [*Patzert*, 1969; *Lumpkin*, 1998; *Dickey et al.*, 2008]. Both types of eddies are accompanied by increased biological production through the upwelling of nutrient rich water from depth, in the cores of cyclonic eddies [*Seki et al.*, 2001; *Bidigare et al.*, 2003; *Kuwahara et al.*, 2008; *Nencioli et al.*, 2008] and around the

peripheries of anticyclonic eddies by submesoscale processes [*Calil and Richards*, 2010].

[3] An example of the eddy field in the region, as represented by sea surface height (SSH) for the week centered on 10 September 2009, is shown in Figure 1a. The SSH is composed of the SSH anomaly from satellite JASON-1 by the AVISO group and the mean SSH of *Niiler et al.* [2003] (hereafter referred to as the altimetry, accessible at http://oceanwatch.pifsc.noaa.gov). Images of earlier times reveal that the major eddies west of the islands all have their origins in the lee of the island of Hawaii. The two anticyclonic eddies marked with 'A' were spun up near 156.5°W, 19°N (marked A_0) in June and August 2009 respectively, and propagated westward. The cyclonic eddy marked with 'C' was spun up near 156.5°W, 20°N (marked C_0) in July 2009. In September 2009, a new cyclonic eddy was spinning up at site C_0.

[4] Generation of the eddies described above can be confirmed with sea surface temperature (SST) as observed by the Geostationary Operational Environmental Satellites (GOES, Figure 1b, data available at http://oceanwatch.pifsc.noaa.gov). A cyclonic eddy may be identified by low SST due to upwelling in its core (e.g., the September cyclonic eddy at C_0) and an anticyclonic eddy is often identifiable by a swirl of warm and cold water if it is spun up in a region

---

[1]International Pacific Research Center, School of Ocean and Earth Science and Technology, University of Hawai'i at Mānoa, Honolulu, Hawaii, USA.

[2]National Institute of Water and Atmospheric Research, Wellington, New Zealand.

[3]Center for Ocean-Atmosphere Prediction Studies, Florida State University, Tallahassee, Florida, USA.

[4]Ocean Dynamics and Prediction Branch, Naval Research Laboratory, Stennis Space Center, Mississippi, USA.
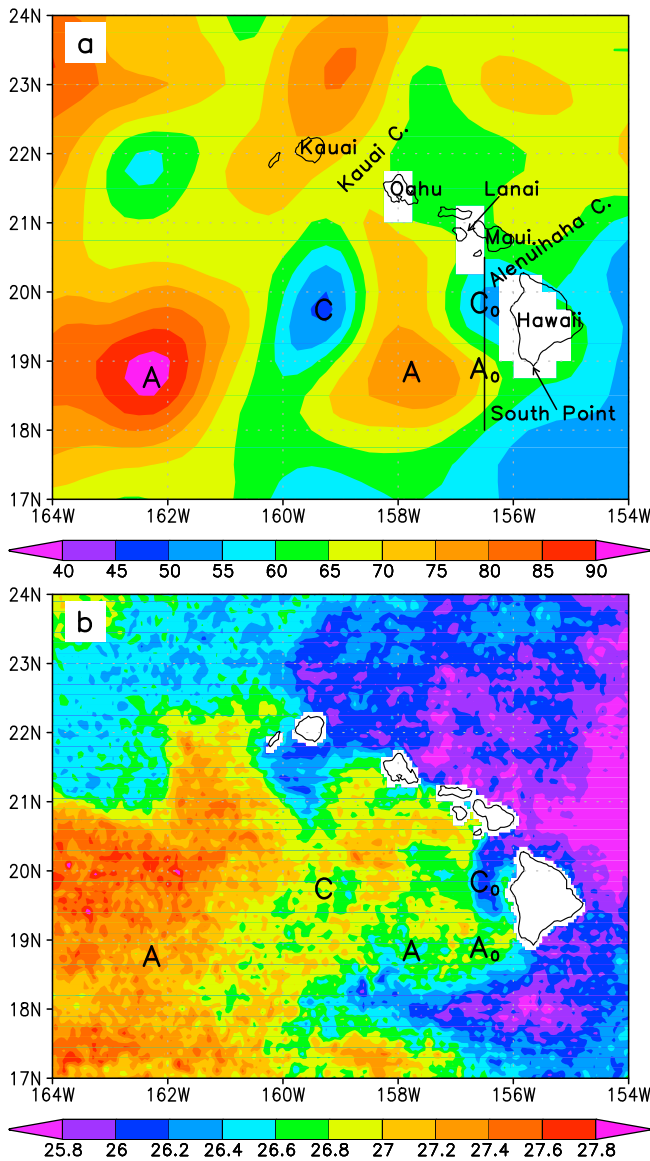
Figure 1. Satellite observations of (a) SSH (cm) composed of the SSH anomaly from satellite JASON-1 by the AVISO group and the mean SSH of *Niiler et al.* [2003] and (b) SST (°C) by the GOES for the week centered on 10 September 2009.

with horizontal temperature contrast (e.g., the August anticyclonic eddy to the immediate west of A_0). In addition, elevated level of concentration of chlorophyll-a (a measure of biological activity), as observed by the Moderate Resolution Imaging Spectroradiometer (MODIS, not shown here), also confirms the formation of these eddies.

[5] The dominance of mesoscale eddies that originate in the lee of the island of Hawaii is well represented in Figure 1. It is possible that eddies of smaller spatial scale, shorter duration and weaker intensity had also been spun up in the lee of the smaller islands during this period but not captured by satellite observations. There had been additional eddy features that either appeared west of the formation sites C_0 and A_0, or arrived from the east around the South Point of the island of Hawaii. By September

2009, these features had all exited the western boundary of the domain in Figure 1.

[6] There are two leading mechanisms on the generation of mesoscale eddies in the lee of an island. The first attributes eddy generation and shedding to an oceanic flow around an oceanic barrier (a deep island), and the second to an atmospheric flow around an atmospheric barrier (a tall island). Both these mechanisms have been demonstrated to operate in the generation of Gran Canaria eddies [*Barton et al.*, 2000; *Basterretxea et al.*, 2002; *Sangrà et al.*, 2007; *Jiménez et al.*, 2008]. In this study, we examine their applicability to the Hawaiian lee eddies with numerical model experiments. The layout of this paper is as follows: a review of the two eddy generation mechanisms and prior studies of Hawaiian lee eddies is presented in section 2; numerical model experiments and results are described in sections 3 and 4; section 5 provides discussions on a number of issues, including the applicability of the two eddy generation mechanisms based on model results (sections 5.1), formation mechanism of the Hawaiian Lee Counter Current (section 5.2) – a revisit and a prelude to section 5.3 in which an interpretation of eddy generation by an atmospheric flow around a tall island is provided, and eddy generation frequency and propagation (section 5.4); a summary of results is given in section 6.

2. Eddy Formation Mechanisms

2.1. Oceanic Flow Around an Oceanic Barrier

[7] The main Hawaiian Islands are on the path of the interior westward flow of the North Pacific subtropical gyre. When the existence of mesoscale eddies in the lee of the Hawaiian Islands was first noted [*McGary*, 1955; *Manar*, 1967], it was natural to attribute their cause to the mechanism of eddy shedding due to an oceanic flow around a barrier. The theoretical basis is the phenomenon of "von Kármán vortex street" [*von Kármán*, 1954], a series of vortices that detach from a cylindrical barrier placed in a steady inertial flow environment.

[8] In a non-rotating frame and homogeneous fluid with a steady unidirectional flow, the nature of flow downstream (or in the wake of) a barrier ranges from laminar to turbulent, usually characterized by the Reynolds number defined as Re = UD/ν where U is the constant upstream flow speed, D is the horizontal scale of the barrier, and ν is the coefficient of molecular viscosity. As the Reynolds number increases, the wake flow transitions from being viscous to inertial. Detachment of vortices occurs as a result of frictional boundary layer separation in the inertial regime at moderate Reynolds numbers, estimated in the range of 40–1000 [*Batchelor*, 1967; *van Dyke*, 1982].

[9] For a stratified fluid in a rotating frame, flow characteristics in the wake become much more complex to describe and require additional measures such as the Rossby number and Burger number in addition to the Reynolds number [*Dong et al.*, 2007]. Nonetheless, in a modeling study of the Gran Canaria eddies that assumes a homogeneous ocean but includes rotation, *Jiménez et al.* [2008] found that a Reynolds number greater than 60 is a good indicator for eddy shedding to occur. Taking a diameter of 54 km for the Gran Canaria and an eddy viscosity of 100 m^2 s^{-1}, the upstream flow speed must be greater than 0.1 m s^{-1}.
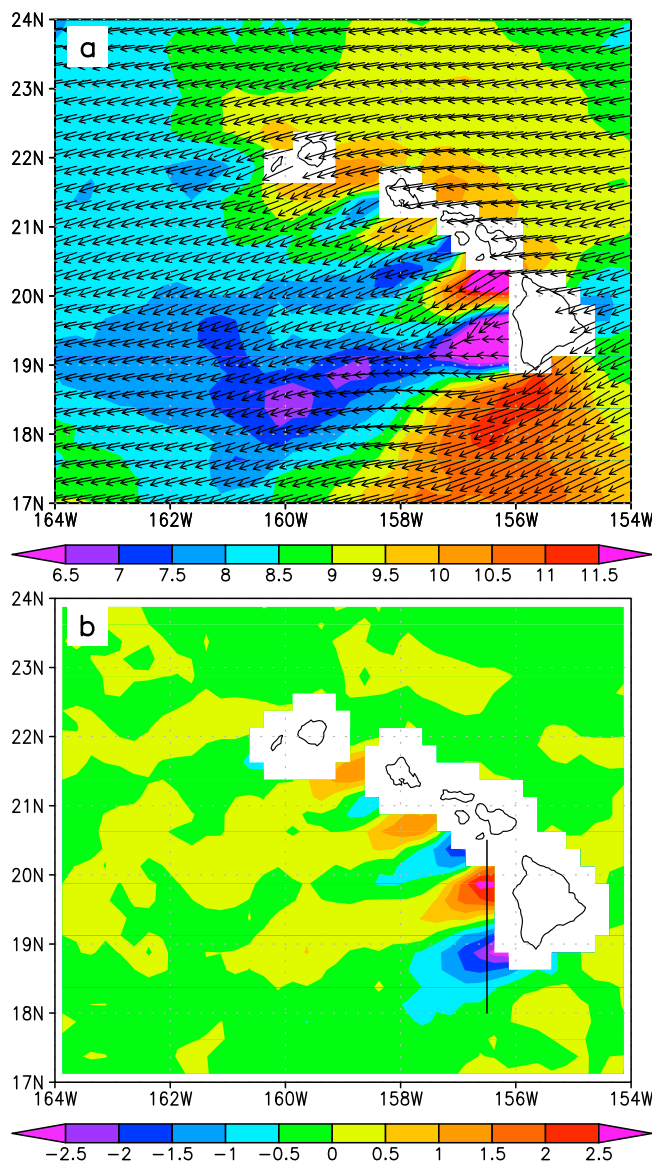
Figure 2. The QSCAT winds averaged over 1–7 August 2009, (a) wind vectors with wind speed in color (m s^{-1}) and (b) wind stress curl (× 10^{-6} Pa m^{-1}).

[10] The earliest extensive study of Hawaiian lee eddies was conducted by *Patzert* [1969] based on historic data collected from 20 cruises. He considered the possibility of eddy generation by an oceanic flow in the lee of the island of Hawaii from several perspectives including Reynolds number. Assuming an upstream flow of 30 cm s^{-1}, a diameter of 150 km for the island of Hawaii, for an eddy viscosity in the range of 1–5 × 10^6 cm^2 s^{-1}, the Reynolds number is in the range of 450–90, which is in the theoretical range for eddy shedding. However, *Patzert* [1969] pointed out that a westward flow of 30 cm s^{-1} was not present in the Alenuihaha Channel during the spin-up of a cyclonic eddy because drifters deployed in the channel did not move significantly westward. Even though the island of Hawaii is a deep-water island, the fact that it is part of a ridge system and is in proximity of the island of Maui (the Alenuihaha Channel is about 24 km wide at its narrowest section) may

result in regional flow characteristics that do not fully conform to the idealized situation of flow around an isolated barrier. Around the South Point of the island of Hawaii, nonetheless, westward flow speed has been observed to reach 1 m s^{-1} at times, thus anticyclonic eddies may be generated there [*Lumpkin*, 1998].

2.2. Atmospheric Flow Around an Atmospheric Barrier

[11] From a rigorous analysis from the standpoint of energy consideration, *Patzert* [1969] concluded that the northeasterly trade winds were the most likely candidate to spin up Hawaiian lee eddies. As an example, the energy required to spin up an intense cyclonic eddy (with a typical flow of 30 cm s^{-1} around the eddy) could be provided by sustained winds of 26 knots (~13 m s^{-1}) for 58 days. This scenario was deemed highly possible based on a mean wind field compiled from 15 years of ships' observations, showing wind vectors of 25 knots in the Alenuihaha Channel. Winds of 30 knots or more were observed in areas of eddy flow on individual cruises.

[12] Observations from a field program, E-Flux, support this mechanism. E-Flux, an interdisciplinary program aimed at an improved understanding of physical, biological, and biogeochemical processes that occur within cyclonic eddies, consisted of three field surveys in November 2004, January 2005 and March 2005 in the immediate lee of the island of Hawaii. Cyclonic eddies, Noah and Opal, were captured in the first and third surveys respectively. During these two periods, the trade winds were persistent and strong (over 35 knots or 18 m s^{-1} at times). No cyclonic eddy was found in the second survey during which period the winds were erratic in magnitude and direction [*Dickey et al.*, 2008].

[13] The prevailing northeasterly trade winds in the region, upon encountering the islands, are funneled through the channels with much acceleration. The fastest atmospheric flow is observed in the Alenuihaha Channel flanked by the tall islands of Maui and Hawaii that represent solid barriers to the atmospheric trade wind layer. This effect is shown clearly by the wind field in early August 2009 as measured by satellite scatterometer, QuikSCAT (hereafter QSCAT, Figure 2a). The wind in the Alenuihaha Channel reaches over 12 m s^{-1}, very close to that used in the energy calculation by *Patzert* [1969]. In addition, acceleration of wind around the South Point of the island of Hawaii is also comparably pronounced. In the lee of each island (or group of islands), a shadow of wind minimum exists. The resulting wind shear drives differential Ekman transport at the ocean surface that, in turn, induces oceanic upwelling in areas of divergence and downwelling in areas of convergence. *Patzert* [1969] hypothesized that cyclonic and anticyclonic eddies form as a result of upwelling and downwelling respectively.

[14] The effect of wind shear on oceanic circulation is best represented by wind stress curl (Figure 2b) which is proportional to Ekman pumping velocity when variations of seawater density and the Coriolis parameter are considered negligible. Dipoles of positive (upwelling) and negative (downwelling) curl appear in the lee of each island group, the strongest being in the lee of the island of Hawaii where strong eddies have been observed to form.
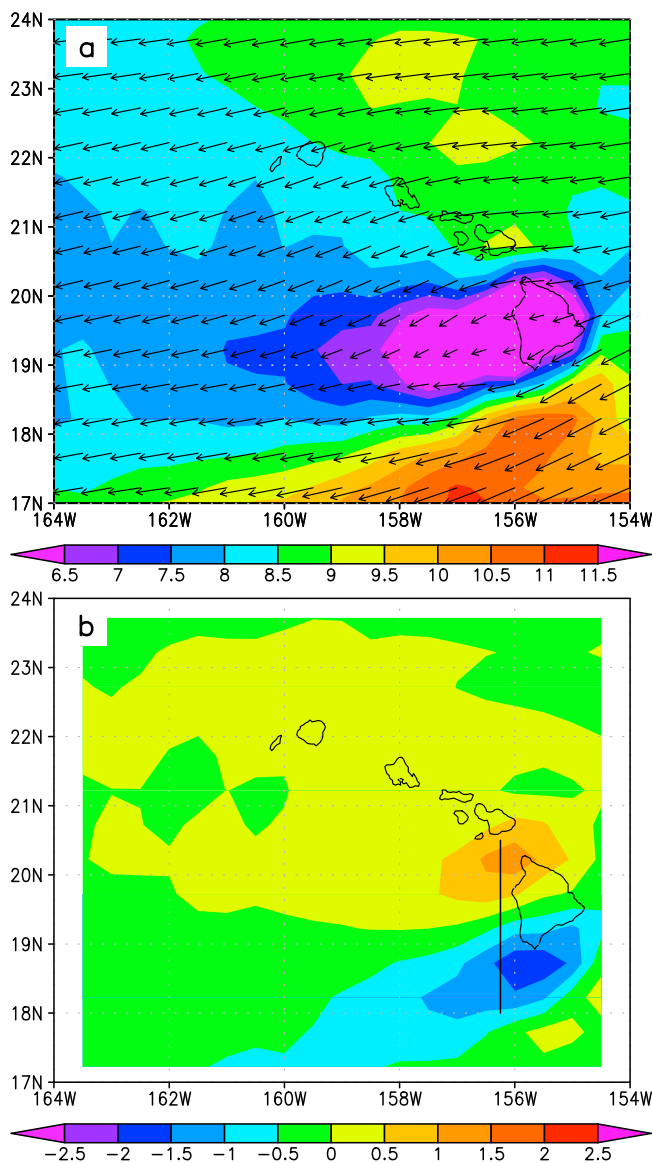
Figure 3. The NOGAPS winds averaged over 1–7 August 2009, (a) wind vectors with wind speed in color (m s^{-1}) and (b) wind stress curl ($\times$ 10^{-6} Pa m^{-1}).

[15] In a numerical modeling study of circulation in the Hawaiian Islands, *Calil et al.* [2008] found that stronger cyclonic eddies were generated when higher spatial and temporal resolution wind-forcing was used to drive the ocean model, which further supports the wind-forcing mechanism. The higher temporal resolution (daily) helps to capture the intensity of the trade winds and the higher spatial resolution (0.25° or finer) is necessary to resolve the details of the wind shear in the lee of the islands. A similar conclusion was also obtained in a similar study by *Kersalé et al.* [2011] with regard to the effect of spatial resolution of wind-forcing. *Kersalé et al.* [2011] also examined the relative importance of wind, current and topography in the generation of Hawaiian lee eddies and suggested that they were all important.

[16] *Jiménez et al.* [2008] conducted a modeling study of the relative importance of wind and current in the generation of Gran Canaria eddies and found that a strong Canary Current (>0.1 m s^{-1}) is sufficient to produce an eddy street but a strong wind can only generate a pair of stationary eddies in the wake of the Gran Canaria. When wind and current are considered concurrently, wind promotes the shedding of eddies starting from a lower Reynolds number of 20, or a weaker upstream current of 0.04 m s^{-1}. This conclusion is supported by observations [*Piedeleu et al.*, 2009].

[17] In the Philippine Islands, *Pullen et al.* [2008] found that strong winds resulting from monsoon surges are capable of causing eddy generation and propagation in the absence of a background current.

3. Modeling Strategy

3.1. The Ocean Model

[18] The Hybrid Coordinate Ocean Model (HYCOM) is implemented for the Hawaii regional domain (166–150°W, 16–26°N). HYCOM is a primitive equation ocean circulation model whose generalized vertical coordinate system allows the freedom to define the vertical grid spacing based on the vertical structure of the ocean, isopycnic (density-following) in stratified ocean interior, level (pressure-following) in unstratified regions such as the surface mixed layer, and sigma (terrain-following) in coastal and shelf seas [*Bleck*, 2002; *Chassignet et al.*, 2003; *Halliwell*, 2004]. This coordinate system is designed to best represent the different dynamic regimes within a single framework [*Chassignet et al.*, 2006].

[19] The Hawaii regional HYCOM is a nested subdomain within an outer model that supplies model fields for initialization and at the lateral boundaries. This outer model is the eddy-resolving global ocean prediction system based on HYCOM and is run in real time at the Naval Oceanographic Office [*Chassignet et al.*, 2009]. Model output is available through the HYCOM Consortium server (http://www.hycom.org). In addition to predicting the future state of the ocean, the global system also provides hindcast analysis through assimilating remotely sensed and in situ oceanographic observations that include surface variables (SSH, sea surface temperature (SST) and sea ice concentration) as well as vertical profiles (CTDs, XBTs and Argo floats), using the Navy Coupled Ocean Data Assimilation (NCODA) system [*Cummings*, 2005]. The global HYCOM/NCODA system has a horizontal resolution of 0.08°, approximately 8.3 km in the Hawaii region. In the vertical, it has 32 hybrid coordinate surfaces. Generally, the deepest 4 surfaces follow closely the ocean bathymetry in the Hawaii region, thus only the upper 28 surfaces are active. Typically, the top 4 surfaces are either pressure-following or terrain-following coordinates spaced at 6 m or less. Transition to density-following coordinates occurs for the deeper surfaces. The bathymetry is based on the Naval Research Laboratory 2′ Digital Bathymetric Data Base 2 (DBDB2) (see D.-S. Ko, NRL DBDB2: Global 2-minute topography, 2002, http://www7320.nrlssc.navy.mil/DBDB2_WWW). The surface wind and thermal fluxes are from the Navy Operational Global Atmospheric Prediction System (NOGAPS) at a resolution of 0.5°.

[20] Configuration of the Hawaii regional HYCOM follows closely that of the global HYCOM with a few modifications. The horizontal resolution of the regional HYCOM
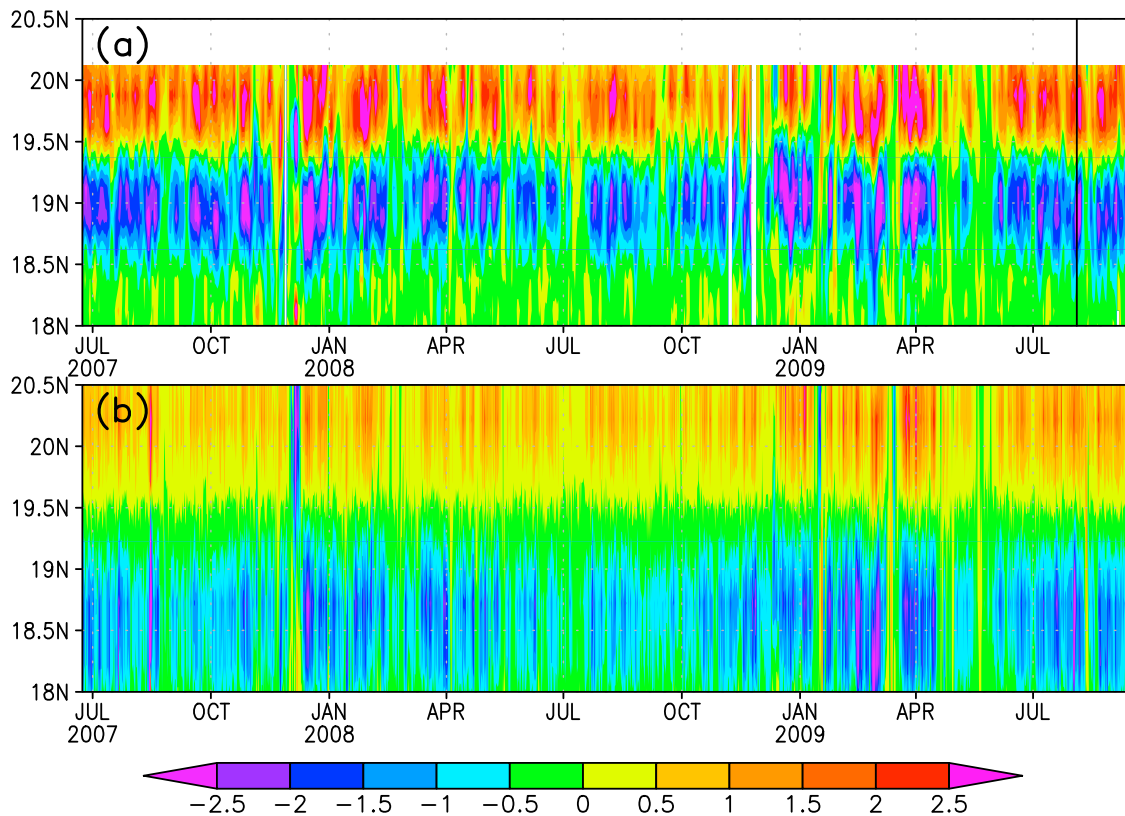
Figure 4. Temporal variation of wind stress curl ($\times 10^{-6}$ Pa m^{-1}), (a) QSCAT along 156.5°W (black line in Figure 2b) with the black line marking 4 August 2009, the center date around which the 7-day mean wind pattern is shown in Figure 2 and is used in experiment STRONG and (b) NOGAPS along 156.25°W (black line in Figure 3b).

is 0.04°(~4 km), a factor of 2 downscaling from the global model. The increased resolution helps to better resolve the major channels, such as the Alenuihaha Channel. The vertical coordinate is the same as that of the global model with the deepest 4 inactive surfaces trimmed off for computational efficiency. The regional bathymetry is created with the General Bathymetric Chart of the Oceans database (GEBCO, 1/60°) and the global model bathymetry as follows (after both are interpolated on to the regional model grid): (1) over a distance of 0.6° inward from the domain's boundaries, the bathymetry matches that of the global model to facilitate the application of boundary conditions; (2) for the interior of the domain, the GEBCO is used to better define the geographic features including the islands' coastline; (3) over a zone of 0.4°, the bathymetry is a weighted average of the global model bathymetry and GEBCO to allow a linear transition from the boundary zone to the interior. A minimum ocean depth of 5 m is set.

[21] Open boundary conditions consist of two parts: the barotropic and baroclinic components. For the barotropic component, the theory of characteristics is applied following *Browning and Kreiss* [1982], which is a well-posed problem. For the baroclinic component, due to the time varying vertical coordinate system of HYCOM, a well-posed mathematical formulation is difficult. Instead, a nudging technique is applied with which the temperature, salinity, layer interface depth and velocity components are restored toward the values from the global model output over a buffer zone of

10 model grid intervals along each boundary (see *Blayo and Debreu* [2005] for a discussion). The restoring time scale increases from 0.2 day at the boundary to 2.0 days over 10 grid points into the interior.

[22] No data assimilation is applied in the regional model. The effects of data assimilation are included only at the initialization and at the lateral boundaries through the use of the global model output.

3.2. Wind Forcing

[23] As in the global HYCOM, we use the NOGAPS surface forcing fields to drive the regional ocean model. In consideration of the effects of winds on the generation of Hawaiian lee eddies, experiments are also performed in which the wind stress was replaced by the satellite derived product QSCAT. Since the QSCAT does not have values near land (see Figure 2), the wind components are first extrapolated to fill the missing points using weighted averages of defined neighboring points in a manner similar to that described by *Kara et al.* [2008], then converted to wind stress using the formula of *Large and Pond* [1981] before interpolation to the model grid. The QSCAT product used in this study has a spatial resolution of 0.25° at daily intervals; each daily product is a composite of 3 days centered on the given day.

[24] Figure 3 displays the NOGAPS mean wind pattern for 1–7 August 2009, which is to be compared with the QSCAT in Figure 2. The most notable feature of the
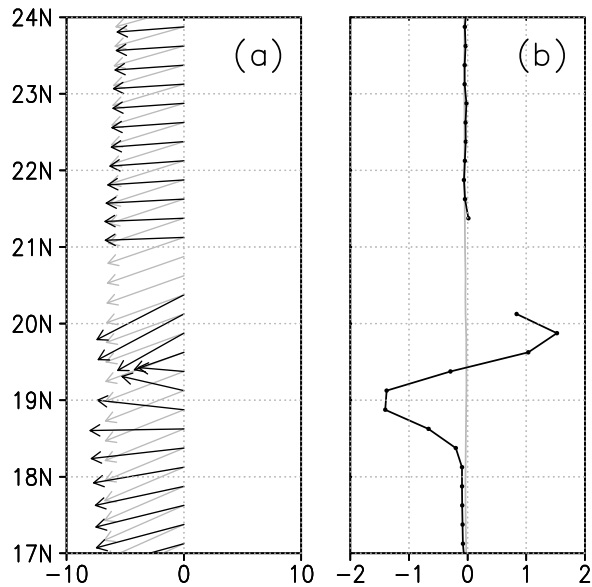
Figure 5. Meridional distribution of time-mean (23 June 2007 to 15 September 2009) (a) QSCAT wind (m s^{-1}) and (b) wind stress curl ($\times 10^{-6}$ Pa m^{-1}). Black: along 156.5°W, in the lee of the island of Hawaii. Grey: zonal-mean (150–140°W), upstream of the model domain, used in experiments Q-MEAN and M-NOHI.

NOGAPS is the broad spatial scale of the wind minimum in the lee of the island of Hawaii (Figure 3a). Acceleration of wind around the South Point is present though the maximum is displaced further south compared with the QSCAT. To the north of the wind minimum, moderate increase in wind speed is present but not related to the individual channels. The resulting wind stress curl (Figure 3b) is a single dipole on a scale that is much broader than the meridional extent of the island of Hawaii. At a resolution of 0.5°, the NOGAPS does not fully capture the effects of the islands on the trade winds.

[25] The temporal evolution of the wind stress curl of the two products for the period of June 2007 to September 2009 is shown in Figure 4. Here we focus on the dipole in the lee of the island of Hawaii, the strongest in the QSCAT and the only one in the NOGAPS. In order to capture the maximum intensity in each of the products, the wind stress curl is displayed along 156.5°W for the QSCAT (the black line in Figure 2b), and along 156.25°W for the NOGAPS (the black line in Figure 3b).

[26] The QSCAT (Figure 4a) shows that the trade wind condition prevails - characterized by positive curl in the northern part of the section and negative curl in the southern part. Cessation of the trade winds does occur from time to time but is usually brief. Inspections of the entire QSCAT record (1999–2009) suggest that the trade winds tend to be strong and persistent during summer and variable during winter, consistent with earlier observations of *Smith and Grubisic* [1993]. For the period considered in this study, however, such a trend is not clear.

[27] The NOGAPS, a numerical weather prediction product that assimilates the QSCAT, captures much of the temporal variation but not the intensity of the wind shear. In

particular, the magnitude of the positive wind stress curl rarely exceeds 2.0×10^{-6} Pa m^{-1}), considerably weaker than that of the QSCAT which exceeds 2.0×10^{-6} Pa m^{-1} often and 2.5×10^{-6} Pa m^{-1} at times.

3.3. Model Experiments

[28] Two main experiments are performed: one employs the NOGAPS surface forcing as in the global HYCOM, and the other uses identical thermal forcing but replaces the wind stress with the QSCAT product. We shall refer to them as experiments NOGAPS and QSCAT respectively. Both are initialized with the global HYCOM fields on 23 June 2007 and integrated to 15 September 2009. The beginning date is the earliest date of the global HYCOM output acquired. The end date is determined by the availability of forcing fields at the time of experiments. The NOGAPS experiment serves two purposes. First, it provides a direct
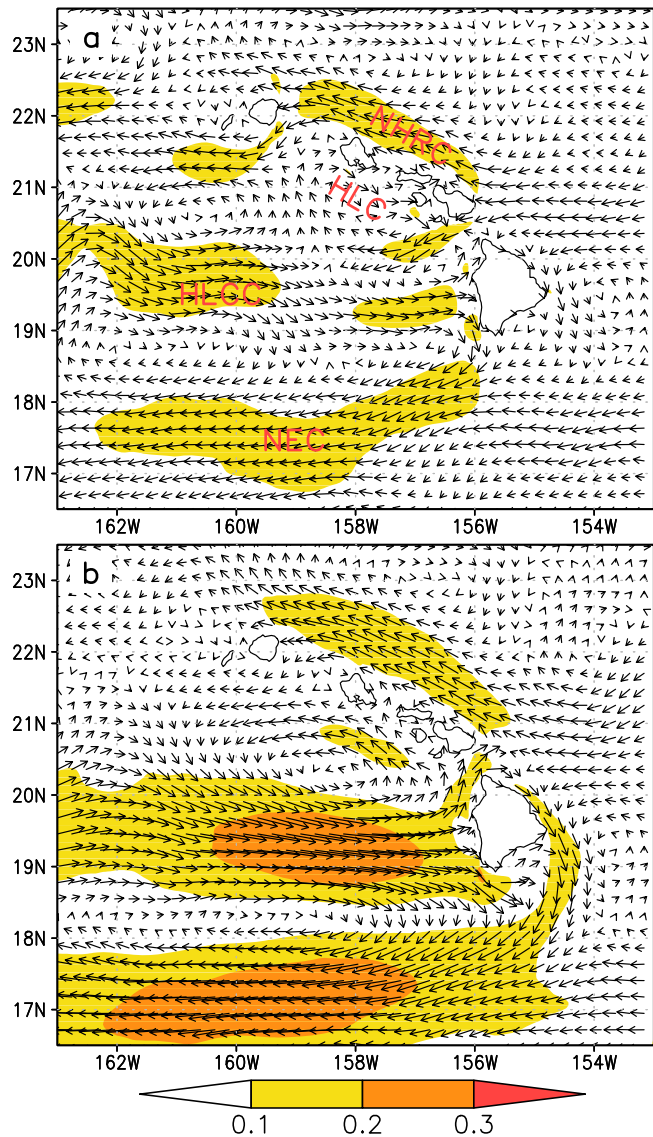

Figure 6. Mean velocity (m s^{-1}) at 50 m averaged over the whole integration period, (a) the QSCAT experiment and (b) the NOGAPS experiment.
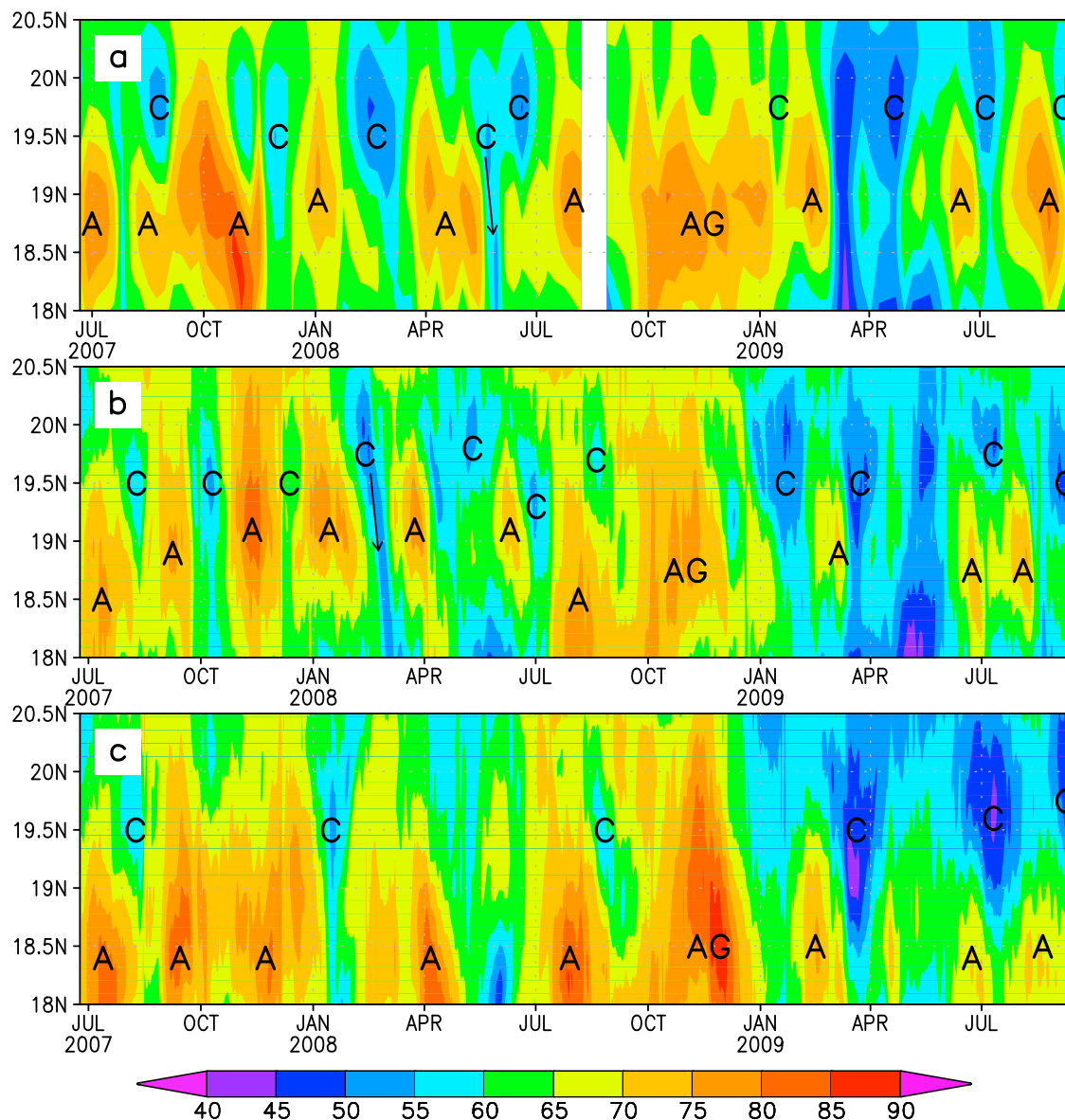
Figure 7. Temporal variation of SSH (cm) along 156.5°W (black line in Figure 1a), (a) the altimetry, (b) the QSCAT experiment and (c) the NOGAPS experiment. The black arrows in Figures 7a and 7b indicate southward propagation of the cyclonic eddies.

comparison of the eddy features found in the non-assimilative model and these obtained when data assimilation is applied in the global HYCOM. Second, the effect of wind-forcing on eddy generation should be revealed when its results are contrasted with that of the QSCAT experiment.

[29] Four auxiliary experiments are also performed, they differ from the main experiment QSCAT as follows: the first, which will be referred to as Q-MEAN, is forced with the time mean (23 June 2007 to 15 September 2009) and zonal mean (150–140°W) of the QSCAT winds as shown in Figure 5; the second, which will be referred to as Q-NOHI, uses a modified bathymetry in which the eight main Hawaiian Islands are submerged to 4000 m below the ocean surface; the third, which will be referred to as M-NOHI, uses the modified bathymetry as for Q-NOHI and the mean winds as for Q-MEAN; the fourth, which will be referred to

as STRONG, is forced with the wind stress pattern as shown in Figure 2.

[30] Figure 5 shows clearly the effects of the island of Hawaii on the trade winds in the lee region (black) compared with the undisturbed wind condition upstream (gray). The upstream wind stress curl is weakly negative whose magnitude in units of 10^{-6} Pa m^{-1} ranges from 0.08 at 26°N to 0.01 at 16°N. The application of this wind pattern in experiment Q-MEAN may be viewed as an idealized case in which the trade winds do not feel the existence of the islands (e.g., a very coarse resolution wind product), thus eliminating the effects of an atmospheric wake on ocean circulation.

[31] The rationale for using the modified bathymetry for experiment Q-NOHI is to explore the regional flow characteristics when the impact of the islands is retained in the
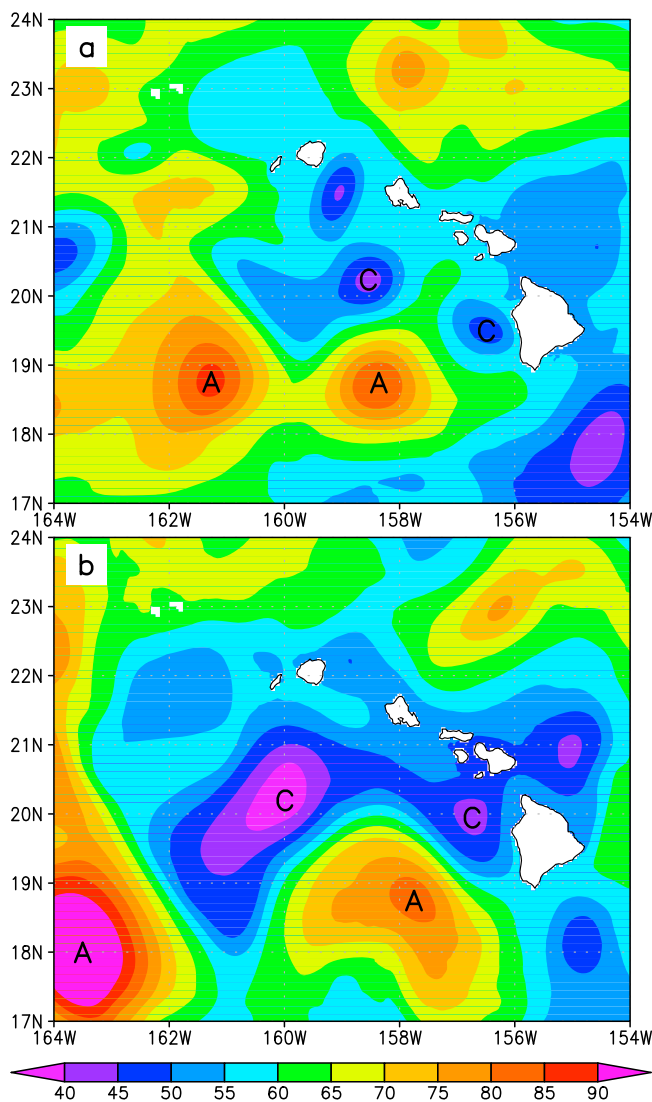
Figure 8. SSH (cm) on 10 September 2009 from (a) the QSCAT experiment and (b) the NOGAPS experiment.

atmospheric forcing but there are no physical barriers to the oceanic flow. Experiment M-NOHI provides a reference point for a typical subtropical ocean gyre circulation without wakes in the atmosphere or in the ocean.

[32] Last, experiment STRONG is designed to explore eddy generation and propagation characteristics under a persistent (constant in time) and strong (see the vertical line marked in Figure 4a) trade wind condition, to compare with results of previous idealized modeling studies.

4. Model Results

4.1. Mean Circulation of the Region

[33] Four major currents exist in this region: the North Hawaiian Ridge Current (NHRC), the North Equatorial Current (NEC), the Hawaiian Lee Counter Current (HLCC) and the Hawaiian Lee Current (HLC). Figure 6 shows the flow fields averaged over the whole integration period at a depth of 50 m from the two main model experiments.

[34] The basin-scale North Pacific subtropical gyre provides the background circulation for this region. The Hawaiian Islands, the visible elements of the Hawaiian Ridge at its southern end, are situated in the path of the westward flow of the gyre interior. *Qiu et al.* [1997] showed, with drifter data, that upon encountering the islands, the westward flow bifurcates into two branches east of the island of Hawaii, the northern branch heads northwestward along the Hawaiian Ridge as the NHRC in a manner of a western boundary current, the southern branch continues westward south of the island as part of the NEC. The HLCC, first identified in surface drifter observations [*Qiu et al.*, 1997], runs eastward toward the island of Hawaii at an average latitude of 19.5°N. Through the analysis of drifter observations, *Lumpkin* [1998] identified the fourth major current of the region, the HLC, which flows northwestward along the southwestern shores of the smaller islands following the Hawaiian Ridge. After passing the island of Kauai, it joins the NHRC as a single current flowing westward along 22°N.

[35] All the major currents appear in the model solutions although their details differ from each other and from drifter observations. Common to both the model solutions, the NHRC exists along the northeastern shores of the smaller islands. The magnitude of this current in both the model solutions is within the observed range of 0.1–0.2 m s^{-1} [*Firing*, 1996; *Qiu et al.*, 1997]. The NEC south of the island is well defined in the QSCAT and in the NOGAPS too except that its northern edge is positioned approximately 0.5° to the south of the South Point. Drifter observations [*Lumpkin*, 1998] show a maximum of 0.2 m s^{-1} at 17.5°N in the mean NEC speed; the modeled NEC is slightly weaker in the QSCAT and stronger in the NOGAPS. The HLCC is a relatively weak current (~0.1 m s^{-1}) with a meridional extent of approximately 1° [*Lumpkin*, 1998]. The HLCC in the QSCAT is consistent with drifter observations whereas it appears broader and stronger in the NOGAPS, running into and wrapping around the island of Hawaii, and the NEC is pushed southward as a result. *Xie et al.* [2001] and *Chavanne et al.* [2002] have attributed the formation of the HLCC to the strongest dipole of the wind stress curl in the lee of the island of Hawaii (Figure 2b), which hints at a connection between this current and the mesoscale eddies in this region. We shall revisit this current in detail in section 5.2. Neither of the model experiments shows a coherent current along the southern flank of the Hawaiian Ridge that can be definitely identified as the HLC. There are, however, elements of northwestward flow in the area, such as the broad flow along the southwestern shores of the smaller islands in the NOGAPS and the westward flow west of Kauai centered at 22°N in the QSCAT. The dynamics of this current is not yet known. We shall, however, discuss its possible connection to the HLCC in section 5.2.

4.2. Eddy Generation in the Lee of the Island of Hawaii

[36] The temporal evolution of the observed SSH along 156.5°W (section marked by the black line in Figure 1a) is shown in Figure 7a, and eddy events that occurred from June 2007 to September 2009 having their origins in the lee of the island of Hawaii are marked. In addition to weekly images of altimetry, the process of identifying these events also involves close inspections of weekly images of GOES SST, 8-day averages of MODIS SST and chlorophyll-a.
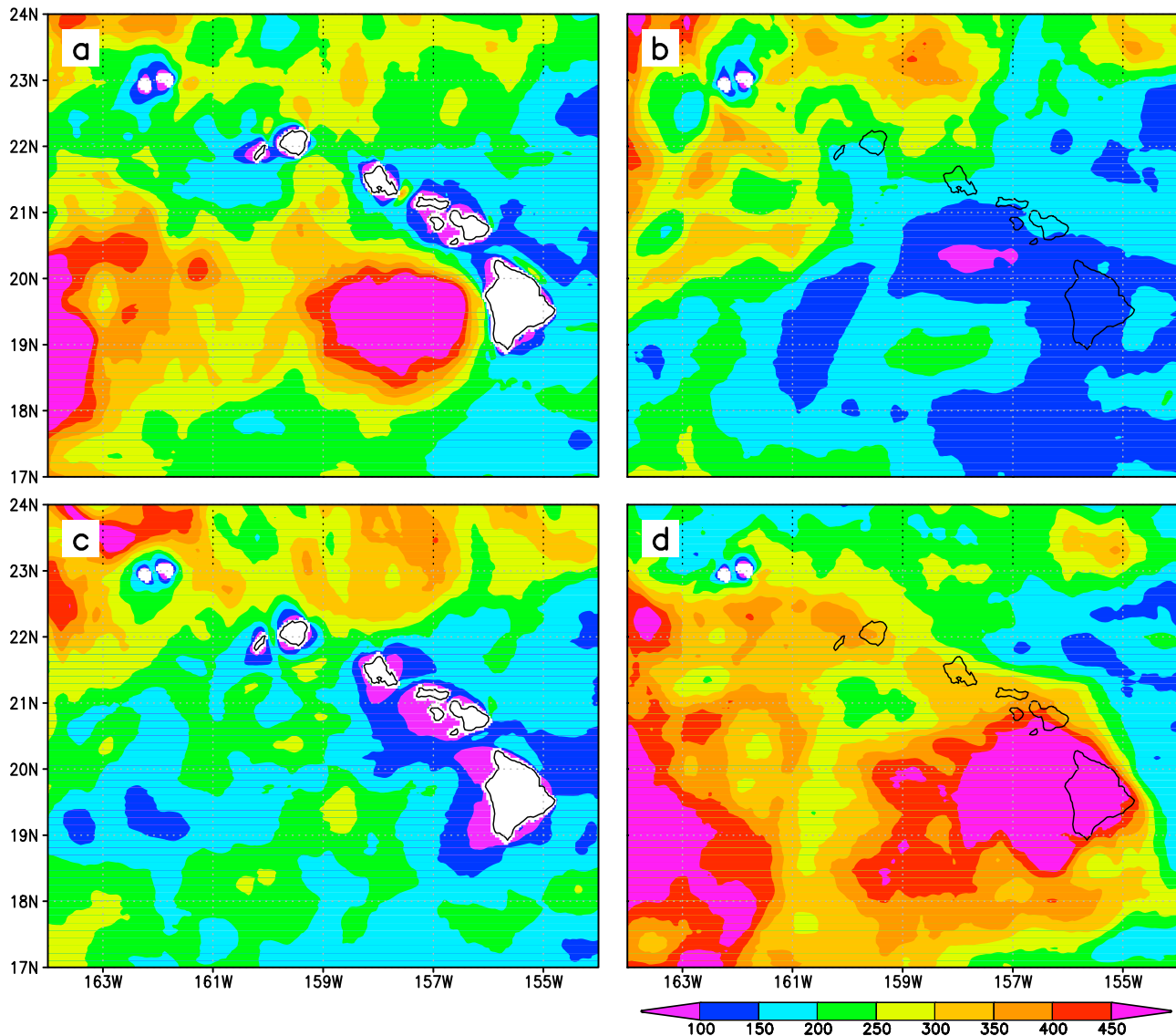
Figure 9. Surface EKE (cm^2 s^{-2}) derived from SSH from (a) the QSCAT experiment, (b) the M-NOHI experiment, (c) the Q-MEAN experiment and (d) the Q-NOHI experiment.

Both objective and subjective criteria are applied. The former includes, for example, signatures of an event must be identifiable for at least two consecutive time levels after leaving its formation site. As an example of the latter, a cyclonic eddy is deemed present if there is a local minimum in SSH accompanied by a minimum in SST and a maximum in chlorophyll-a without using a predefined threshold in each of the variables. Due to the relatively coarse sampling resolutions of these remotely sensed products, it is highly likely that some eddies are not captured (see discussions by *Sangrà et al.* [2009] and *Dong et al.* [2009]), thus eddy occurrences as displayed in Figure 7a should be considered as one estimate at the lower of a possible range instead of a definitive account.

[37] The temporal variations of SSH along 156.5°W in the two main model experiments are shown in Figures 7b and 7c. Several remarks can be made: (1) eddies are generated frequently, and with a few exceptions, cyclonic and anti-cyclonic eddies appear in an alternating manner in the altimetry and the QSCAT experiment; (2) more eddies are generated in the QSCAT experiment and fewer in the NOGAPS experiment than in the altimetry, this is especially true for cyclonic eddies and for the period up to September 2008; (3) for the period of October to December 2008, high SSH dominates the lee of the island in a manner that resembles an anticyclonic gyre (marked 'AG') occupying the area east of 161°W and south of 20°N rather than an isolated mesoscale eddy, this behavior is exhibited by the altimetry data and the model solutions; and (4) with the exception of the first cyclonic eddy in 2009 that is absent in the NOGAPS experiment, both the model experiments reproduce the eddy events that are present in the altimetry for the period of January to September 2009 even though the timing of these events do not match precisely.

[38] The eddy field on 10 September 2009 as produced by the model experiments are shown in Figure 8 which is to be
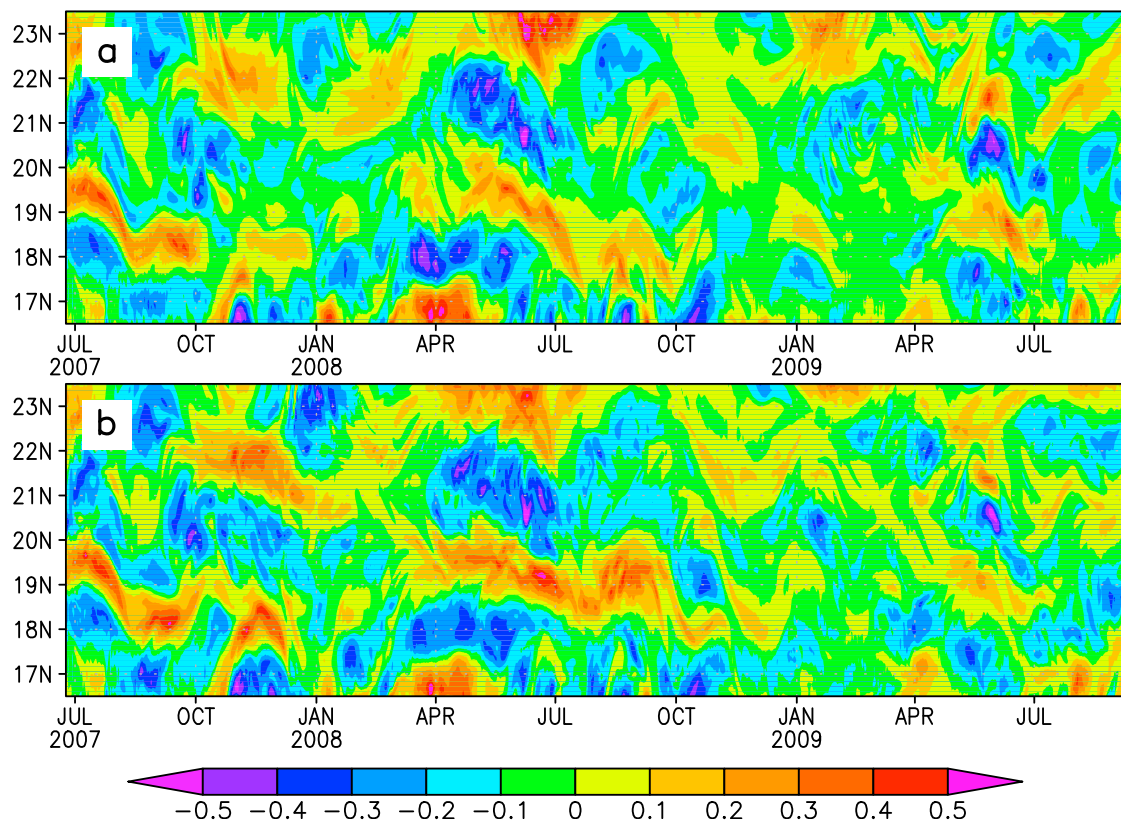
Figure 10. Temporal variation of eastward velocity (m s^{-1}) at 50 m along 154°W (a) in the Q-MEAN experiment and (b) in the QSCAT experiment.

compared with the altimetry data shown in Figure 1a. The eddies generated from June to September 2009 are present in the domain in the model solutions although their locations do not match well that in the altimetry. The mismatch in location is a result of different eddy propagation behavior and eddy shedding time. For example, eddy propagation seems to be the factor in case of the June anticyclonic eddy since the shedding time (end of June) is common to the altimetry and the model experiments (see Figure 7). In the QSCAT experiment, this eddy propagates westward in a relatively steady rate initially. In late August, however, it takes a northward diversion from 18°N to 19.5°N and then retreats southward in early September, which has resulted in its slightly more eastward position in Figure 8a. In the NOGAPS experiment, this eddy simply propagates fast and steadily, hence its more westward position in Figure 8b. For the August anticyclonic eddy, eddy shedding time appears to be the cause. It is shed about a week earlier in the QSCAT experiment than in the altimetry and the NOGAPS experiment, which has resulted in its slightly more westward position in Figure 8a.

[39] The global HYCOM SSH field on 10 September 2009 (not shown) resembles the altimetry in Figure 1a. In fact, the global HYCOM SSH follows the altimetry most of the time in terms of showing the presence of eddy features in the lee of the Hawaiian Islands. However, the evolution of each eddy (spin-up and propagation) is not always captured consistently. At times, certain features disappear from the solution and then reappear again later with their revised positions. This behavior suggests that the eddy field in the global HYCOM is determined primarily through data assimilation.

5. Discussion

5.1. Eddy Variability

[40] In this section, we examine the relative contributions of oceanic and atmospheric island wakes to eddy variability in terms of eddy kinetic energy (EKE) making use of the main experiment QSCAT and the three auxiliary experiments Q-MEAN, Q-NOHI and M-NOHI.

[41] The surface EKE evaluated from the SSH for the four model experiments is shown in Figure 9. The most striking feature of the EKE in experiment QSCAT (Figure 9a) is the high level of intensity (>450 cm^2 s^{-2}) to the immediate west of the island of Hawaii. This pattern is also obtained from multiyear altimetry by *Calil et al.* [2008] with a lower maximum (~400 cm^2 s^{-2}). The higher EKE in the QSCAT than that derived from altimetry may not be unreasonable considering the relatively coarse sampling resolution of altimetry in space and time. In contrast, no such regional enhancement exists in experiment M-NOHI (Figure 9b) in which neither atmospheric nor oceanic wake is included, yielding a background EKE less than 250 cm^2 s^{-2}. By comparison, oceanic wake that is included in experiment Q-MEAN makes a very small contribution to the overall eddy energy (Figure 9c), only marginally higher than the background level in a broader region west of the islands;
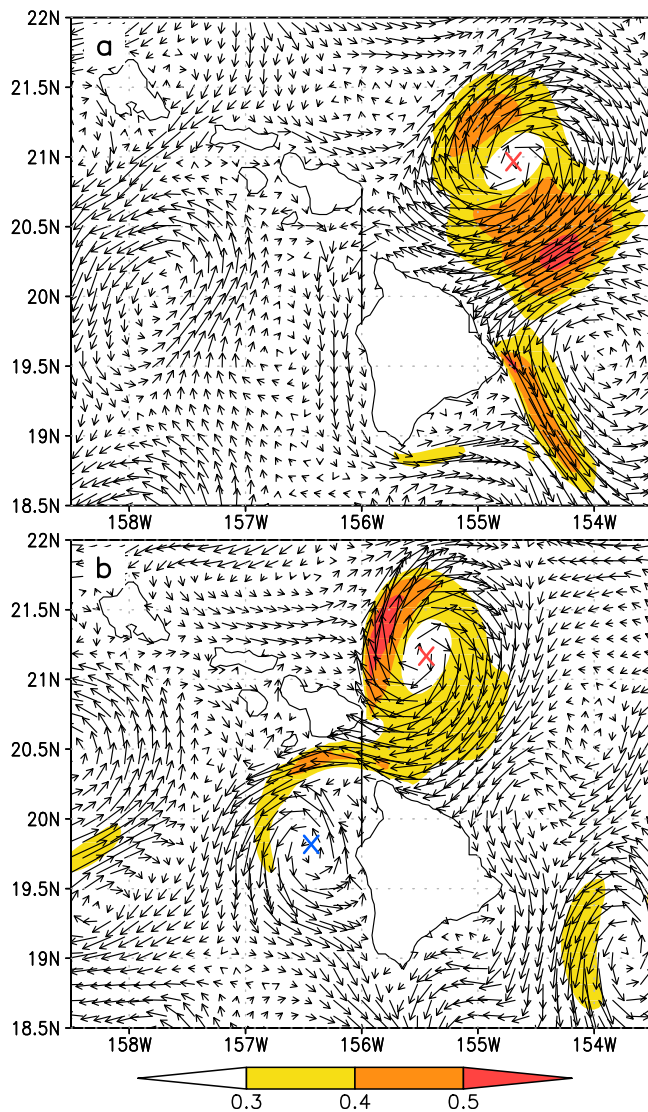
Figure 11. Velocity (m s^{-1}) at 50 m of the Q-MEAN experiment on (a) 5 June and (b) 25 June 2009. Red 'x' marks the center of the passing anticyclonic eddy, and blue 'x' marks the center of the developing cyclonic eddy.

whereas the atmospheric wake that is included in experiment Q-NOHI has produced an overwhelming level of eddy energy (Figure 9d), and in the absence of the islands, the elevated EKE region (>300 cm^2 s^{-2}) has expanded in all directions with an northeastward shift in the location of the maximum(>450 cm^2 s^{-2}).

[42] Figure 9 shows that the EKE level in Q-MEAN is too low to account for the observed regional enhancement in the lee of the island of Hawaii. This is because eddies are spun up in the island lee infrequently and with weak intensity in this experiment. There is a lack of coherent westward flows through the Alenuihaha Channel and around the South Point to promote eddy shedding. The flow field east of the island is highly variable as shown in Figure 10a (Figure 10b is for experiment QSCAT, included here to show that the flow characteristics are similar in the two experiments despite the different wind products used.). At times, propagating features from the east may induce strong eastward flows (>0.3 m s^{-1})

through the Alenuihaha Channel and around the South Point which in turn may induce eddy generation in the lee of the island. Examples are shown in Figure 11 that captures the formation of a cyclonic eddy by a strong channel flow resulting from a passing anticyclonic eddy upstream, and in Figure 12 that depicts the spin-up of an anticyclonic eddy by a passing cyclonic eddy around the South Point. These two eddies are the strongest ones among those formed in this experiment (approximately 6 in each type).

[43] The high EKE level of an expanded horizontal scale in Q-NOHI may seem excessive but is consistent with the extrapolation of the wind field to cover the regions occupied by the submerged islands (and consequently an expansion of the atmospheric wake). Eddies in this experiment tend to be larger and stronger on average than in the main experiment QSCAT. Figure 13a shows the spin-up of a pair of eddies
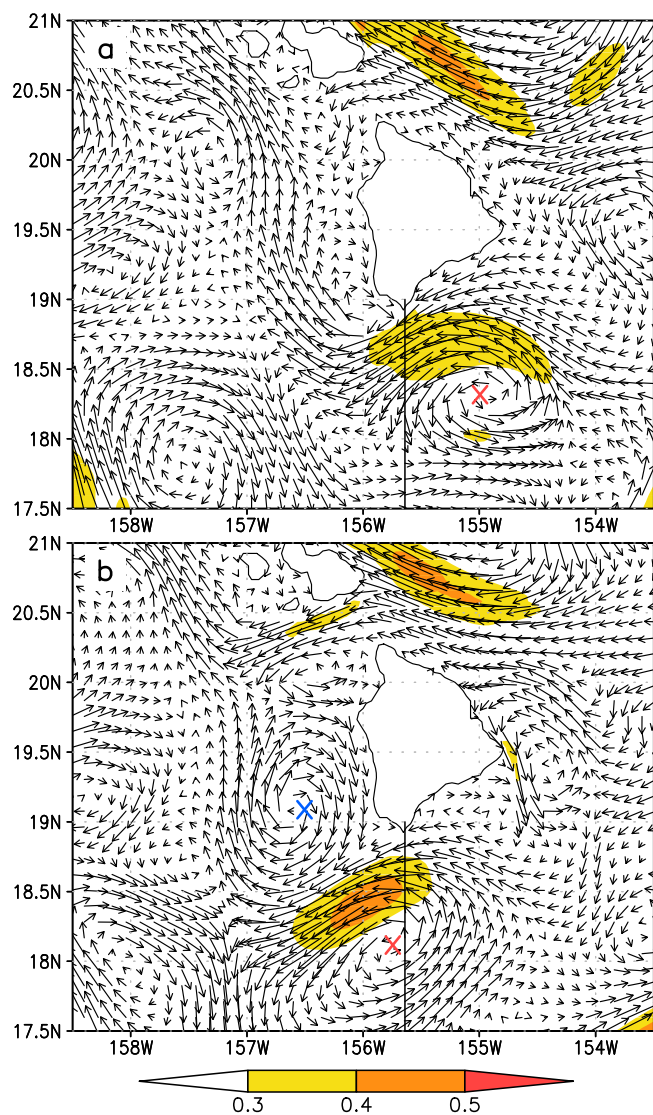

Figure 12. Velocity (m s^{-1}) at 50 m of the Q-MEAN experiment on (a) 20 October and (b) 30 October 2007. Red 'x' marks the center of the passing cyclonic eddy, and blue 'x' marks the center of the developing anticyclonic eddy.
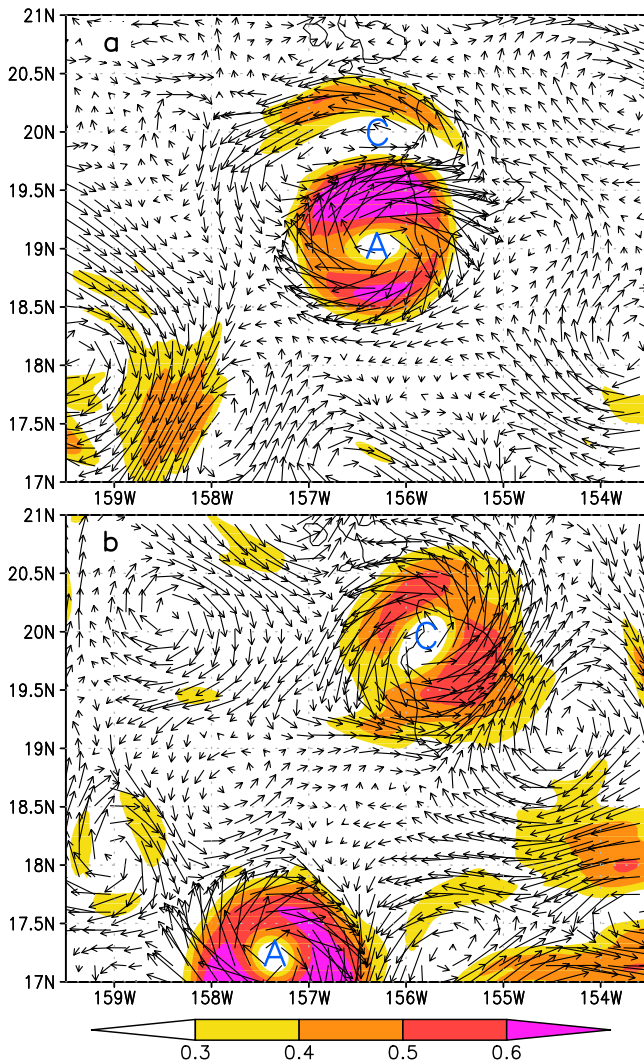
Figure 13. Velocity (m s^{-1}) at 50 m of the Q-NOHI experiment on (a) 22 January and (b) 22 March 2008.

west of and partially over the region occupied by the island of Hawaii. After some further growth, the anticyclonic eddy moves away from the formation site, propagating in a southwestward then westward direction after an initial eastward drift (Figure 13b). The cyclonic eddy strengthens in the meantime, and then propagates northwestward along a path coinciding with the submerged Hawaiian Ridge before turning westward. The eddy flows are significantly stronger than their surroundings, indicating that they are fueled by an external energy source (wind in this case), and they remain strong in their westward passage of 4 to 5 months to reach the western boundary of the model domain. This is in sharp contrast to the developing eddies in Figures 11 and 12 that draw energy from the stronger oceanic flows nearby with a much shorter life span of about one month.

5.2. The Hawaiian Lee Counter Current

[44] In this section, we revisit the formation mechanism of the HLCC by the dipole of the wind stress curl in the lee of the island of Hawaii as proposed by earlier studies [*Xie et al.*, 2001; *Chavanne et al.*, 2002], and make con-

nections between wind stress curl and source/sink in inducing oceanic flows, serving as a prelude to an interpretation of eddy generation by the same mechanism to be discussed in the next section.

[45] *Chavanne et al.* [2002] constructed a flow field for the Hawaii region based on Sverdrup balance using a wind field at 25 km resolution derived from the National Aeronautics and Space Administration scatterometer (NSCAT) measurements. The NSCAT wind pattern is very similar to the QSCAT (Figure 2). In addition to the eastward current at 19.5°N, the HLCC, there was also a weaker eastward current at 20.5°N corresponding to the dipole in the lee of the group of 4 islands north of the Alenuihaha Channel. Both the currents extended westward from the islands to the western boundary. The weaker dipoles of wind stress curl in the lee of the islands further north did not result in eastward flows.

[46] *Xie et al.* [2001] reproduced an eastward current in the solution of a numerical model simulation that used the wind product from the European Centre for Medium-range Weather Forecast (ECMWF) analysis. The ECMWF wind stress curl field at 1.125° resolution contains just one broad dipole over the islands, a pattern very similar to the NOGAPS (Figure 3b). The eastward current in the model simulation was a response to the broad dipole and therefore had a much wider meridional extent than observed. Again, the current extended all the way to the western boundary.

[47] Despite the apparent differences in oceanic circulation presented by *Xie et al.* [2001] and *Chavanne et al.* [2002], the mechanism for the formation of an eastward current by a dipole of wind stress curl is common to both the studies. Generically this is the same as flows induced by sources and sinks, also known as the β-plume effect [*Stommel*, 1982]. A source (sink) could be a direct injection (extraction) of mass into (out of) the system, or in the form of a mass flux from one density layer to another. In Figure 2b, areas of positive wind stress curl (northern part of the lee of each island group) represent sinks to the ocean interior, that is, mass is lost to the surface Ekman layer through upwelling. Conversely, regions of negative wind stress curl represent sources to the ocean interior. Such a mechanism is used by *Jia* [2000] to explain the existence of the eastward flowing Azores Current in the North Atlantic subtropical gyre. We reiterate the arguments here.

[48] *Pedlosky* [1996] showed that, for a localized source or sink of finite extent situated some distance away from the lateral boundaries, zonal flows are induced west of and within the latitudinal band of the source or sink. The zonal flows are bi-directional under the constraint of zero pressure gradient to the east of the source or sink and outside the latitudinal band containing the source or sink. In case of a sink, there is a larger eastward flow toward the southern part of the sink and a smaller westward flow away from the northern part of the sink. Flow directions are reversed in case of a source but the southern branch remains as the larger one. The transport of each of the zonal flows is large in relation to the strength of the source or sink, but the difference in the zonal flows equals to the strength of the source or sink, to satisfy mass conservation [*Pedlosky*, 1996, pp. 405–409]. Such a flow pattern was obtained in laboratory experiments [*Stommel et al.*, 1958] and model solutions [*Luyten and Stommel*, 1986]. For a given source or sink, this
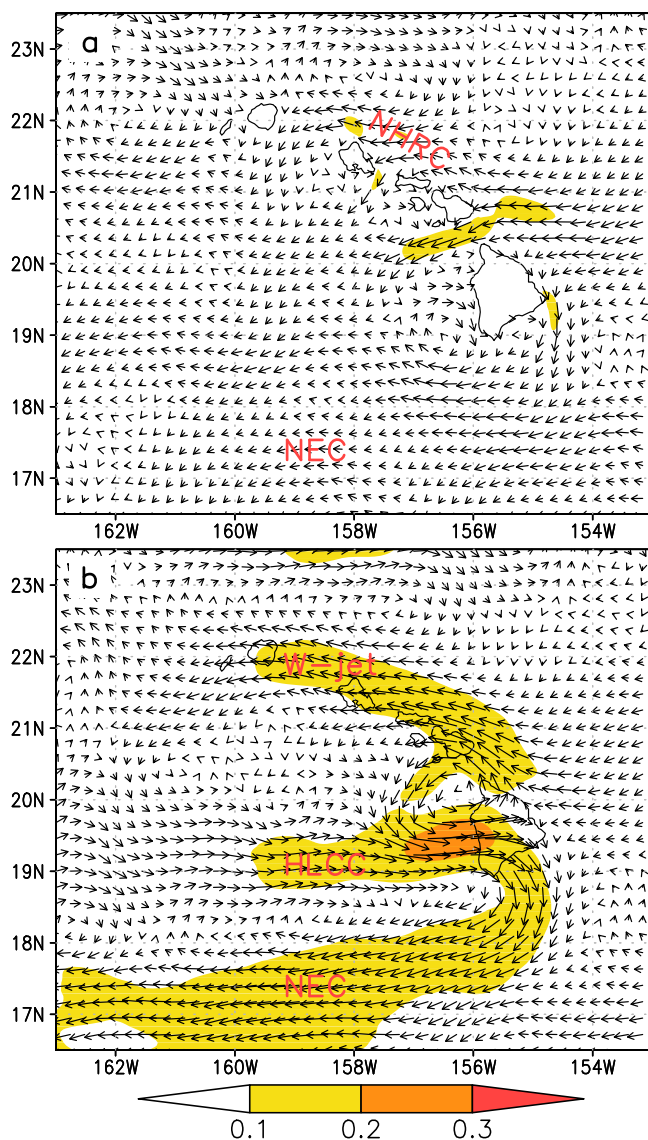
Figure 14. Mean velocity (m s^{-1}) at 50 m averaged over the whole integration period, (a) the Q-MEAN experiment and (b) the Q-NOHI experiment.

an eastward jet running toward the island flanked by westward jets to the north and south. The eastward jet would be the HLCC, its northern part and the westward jet to its north are induced by the sink (positive wind stress curl) and its southern part and the westward jet to its south are responses to the source (negative wind stress curl). The solutions of the QSCAT and NOGAPS experiments confirm such a circulation pattern (Figure 6). In particular, the wider HLCC in the NOGAPS than in the QSCAT is consistent with the broader spatial scales of the dipole of the wind stress curl in the NOGAPS than in the QSCAT (Figures 2b and 3b). The westward jet south of the HLCC joins the NEC; the enhancement of the NEC to the west of the island of Hawaii in both the model solutions is indicative of this additional contribution. Furthermore, without a dipole of the wind stress curl in the lee of the island of Hawaii in experiment Q-MEAN, the HLCC is absent and the NEC is considerably weaker than in experiment QSCAT (compare Figures 6a and 14a).

[51] The westward jet north of the HLCC, narrow and with limited westward extension in the QSCAT, wider and with further westward extension in the NOGAPS, is also consistent with the distribution of the wind stress curl in each experiment. Although this westward jet is an expected response to the positive wind stress curl, no zonal jet is observed north of the HLCC. This could be due to a lack of adequate oceanic observations in the lee of the islands. Another possibility is that the HLC is the expected westward current that has acquired a northward component from the northwestward propagating cyclonic eddies originating in the lee of the island of Hawaii (see section 5.4 for a discussion on eddy propagation), and that the detection of the HLC requires long-term observations to capture a sufficient number of such eddies. The relatively short integration length (~2 years) of the model experiments may have resulted in the less than well defined HLC in the solutions. One indication to support this possibility is shown in the mean flow pattern of experiment Q-NOHI (Figure 14b). In this experiment, a strong westward flow (marked as W-jet) runs along the submerged ridge. Since there are no physical barriers to the oceanic flow in this experiment, the W-jet is not the NHRC. Rather it is the combination of the westward flow resulting from the positive wind stress curl and the upstream westward flow that would have become the NHRC if the main Hawaiian Islands had not been submerged. This is in sharp contrast to experiment M-NOHI in which the upstream westward flow continues over the broad region of the submerged islands in the absence of the dipole of the wind stress curl and the main Hawaiian Islands (not shown).

[52] It is worth noting that even the HLCC, induced by both the source and sink (the dipole of wind stress curl), is identifiable only in long-term mean observations and does not extend all the way to the western boundary. *Yu et al.* [2003] showed that mesoscale variability limits the westward extension of the HLCC to 175°W by drawing energy from mean flow. This may also be the reason why there are no multiple zonal jets present in the lee of the smaller islands in the QSCAT experiment (Figure 6a) despite the dipoles of wind stress curl (Figure 2b), these northern dipoles are too weak to cause notable effects on the highly variable flow field of the region.

theory predicts the upper limits on the strength of the zonal flows.

[49] The eastern boundary ventilation theory of *Pedlosky* [1983] sets the lower limits on the strength of zonal flows induced by sources and sinks. A downward mass transfer at the eastern boundary results in an eastward flow into the boundary (the sink) in the upper layer and a westward flow out of the boundary (the source) in the lower layer. The flow is uni-directional in each layer and its transport equals to the mass transfer, a case of simple mass balance.

[50] The sources and sinks in Figures 2b and 3b have finite extent and are attached to the eastern boundary (the islands). We may envisage multiple zonal flows in the lee of the Hawaiian Islands of varying strength within the limits set by *Pedlosky* [1983, 1996]. In the lee of the island of Hawaii, bi-directional flows are induced by the source and sink (the strongest dipole of wind stress curl), and we expect

5.3. Oceanic Eddy Generation and Shedding by an Atmospheric Wake

[53] Here we consider how oceanic mesoscale eddies, such as the Hawaiian lee eddies, may be induced by wind stress curl resulting from an atmospheric wake, or source and sink in a generic definition, drawing upon findings of *Davey and Killworth* [1989] and *Aiki and Yamagata* [2000]. Both studies considered flows produced by discrete sources with a horizontal length scale comparable to the local Rossby radius in reduced gravity layer models. Results can be summarized in terms of three flow regimes as follows: (1) the Rossby wave regime when the source is very weak ($\leq 5 \times 10^{-2}$ Sv), the oceanic response is a linear Rossby wave extending westward from the source with meridional flow in the forced region only and pure zonal flows (bi-directional) to the west of it; this flow pattern is the same as that described by *Pedlosky* [1996]; (2) the weakly nonlinear regime when the amplitude of the forcing (source) is increased (but still $\leq 8 \times 10^{-2}$ Sv), the response is a series of shed weak eddies that are not fully separated from each other; the eddies travel westward at a speed that is faster than the advancing Rossby wave in the linear regime; (3) the strongly nonlinear regime when the strength of the source is much increased ($>8 \times 10^{-2}$ Sv), the ocean responds with strong isolated lenses of greater amplitude, larger radius and faster westward propagation than the weakly nonlinear regime; this regime is applicable to, for example, the formation of meddies [*Armi and Zenk*, 1984] by the injection (~1 Sv) of the dense and salty Mediterranean Water in the North Atlantic. In both the studies, the forcing (source) is steady throughout the entire integration period (800 days for *Davey and Killworth* [1989] and 1000 days for *Aiki and Yamagata* [2000]).

[54] The quantitative relationship between the strength of the source and the circulation regime may not translate directly from a reduced gravity model to a primitive equation ocean circulation model. Nonetheless, the finding that the source must be sufficiently strong in order for eddy shedding to occur is consistent with observations of eddy generation in the lee of the island of Hawaii during periods of strong trade winds such as cyclonic eddies, Noah and Opal, captured during the E-Flux I and III surveys [*Dickey et al.*, 2008]. The apparent lack of eddy generation in the lee of the smaller islands in observations may be attributed to the weaker dipoles in the wind stress curl, and so is the absence of eddy formation in the lee of the island of Hawaii during weak-trade or no-trade wind conditions (e.g., E-Flux II survey).

[55] The persistence of the trade winds as shown in Figure 4a may be regarded as a pseudo steady forcing except for the periods of September to November 2008 and May 2009 when the trade winds are variable. The former period almost coincides with the time (October to December 2008) when the circulation in the island lee is in the form of an anticyclonic gyre instead of eddies, and there is no eddy event in the latter period in the altimetry data and in the model solutions (Figure 7). The circulation pattern during these periods may be considered in the linear regime of *Davey and Killworth* [1989] and *Aiki and Yamagata* [2000]. For the rest of the integration period, eddy shedding is frequent and is consistent with the nonlinear regimes even though there are discrepancies in the shedding frequency among the altimetry data and the model solutions.

[56] The close relationship between wind and eddy is revealed more clearly when individual eddies are examined. In the QSCAT experiment, for example, the spin-up of the cyclonic eddy in January 2009 is not gradual. During the first 8 days of January 2009, cyclonic circulation develops southwest of the Alenuihaha Channel in response to the strong trade wind burst (Figure 4a). The cyclonic circulation weakens when the trade winds cease in the following 10 days. When the trade winds return later in the month, the cyclonic circulation strengthens, leading to the formation of the cyclonic eddy. Even though the trade winds are interrupted again on 28–29 January, the eddy is sufficiently strong by then to retain its coherence. The altimetry data shows a weak cyclonic eddy during that time. In the NOGAPS experiment, no cyclonic eddy is shed but a cyclonic gyre circulation is present at that time, which is likely the result of the interrupted trade winds that are also weaker than in the QSCAT. All the eddy occurrences after the cyclonic eddy in January 2009 follow closely the periods of intense trade winds in each of the model experiments despite the fact that their times do not match precisely that in the altimetry (e.g., the anticyclonic eddy in February 2009 forms a little later and the one in August 2009 forms a little earlier in the QSCAT experiment than in the altimetry data). Note that eddy onset times can only be approximately determined from the altimetry data because of its weekly sampling resolution. Further, in addition to the absence of a cyclonic eddy in January 2009 in the NOGAPS experiment, there are also fewer cyclonic eddy events prior to that time, which is consistent with the generally weaker positive wind stress curl in Figure 4b.

[57] Observations of eddy generation in the lee of the smaller islands are rare but they do exist. An anticyclonic eddy in the lee of Oahu was captured by high-frequency Doppler radio current meters [*Chavanne et al.*, 2010] in October 2002 and lasted for about 2 weeks; and one cyclonic eddy was reported to shed in the lee of Lanai in December 2007 and lasted for about 9 days [*Dong et al.*, 2009]. Neither is evident in the altimetry. These small and shorted lived eddies are unlikely to be resolved by satellite altimetry due to the relatively coarse sampling resolution in space and time. In the QSCAT experiment, however, a weak cyclonic eddy is present in the lee of Lanai (marked by 'x' in Figure 15a) for about 10 days in December 2007 without propagation. The trade winds were strong for about 20 days toward the end of 2007. In fact, weak eddies of both signs often form in the lee of the smaller islands in the QSCAT experiment when the trade winds are strong. Figure 15b shows the presence of 4 small-scale features in the lee of the smaller islands, in response to a period of strong and persistent trade winds in August 2008. None of these features is evident in the altimetry. In the NOGAPS experiment, small eddy features also form around the smaller islands but the sites and times of formation are variable. It is worth noting that small features do not always appear as clearly as shown in Figure 15b in the QSCAT experiment under strong trade winds. Usually, some are more evident than others. Also most of them do not move far or last long before losing their identity either by dissipation or merging into stronger features of the same sign. It is possible that the model resolution is not sufficient to adequately resolve such small scale features. Since the original QSCAT winds do not
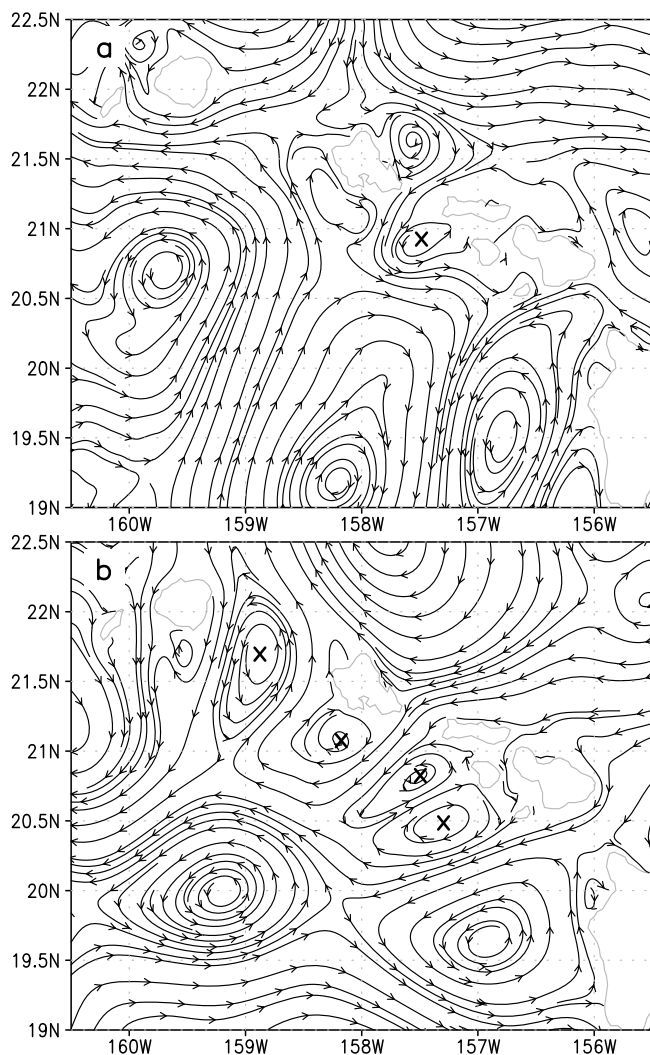
Figure 15. Circulation pattern at 50 m of the QSCAT experiment on (a) 20 December 2007 and (b) 20 August 2008. Small-scale eddies in the lee of the smaller islands are marked with 'x'.

cover the nearshore areas of the islands (Figure 2), it is also possible that the extrapolation of the QSCAT winds into the shores does not capture the intensity of actual winds around islands.

5.4. Eddy Generation Frequency and Propagation

[58] In the nonlinear regimes of *Davey and Killworth* [1989] and *Aiki and Yamagata* [2000], the time scale to generate an eddy is the time taken for the eddy to propagate westward across the forced region. Once an eddy has moved away from the forced region, a new eddy begins to form, thus the frequency of eddy generation is closely linked to the speed of eddy propagation. They also show that eddy propagation speed depends on the strength of the forcing (or nonlinearity). In the case of a 2.5-layer reduced gravity model of *Aiki and Yamagata* [2000], eddies in the weakly nonlinear regime propagate slightly faster than the second long Rossby wave which is the dominant advancing Rossby wave in the linear regime. In the strongly nonlinear regime, the isolated eddies propagate much faster than the non-

isolated eddies in the weakly nonlinear regime. The stronger the forcing, the faster the isolated eddies propagate. At a mass source of 1 Sv, eddies travel at a speed that is more than 4 times of the second long Rossby wave.

[59] The numerical results of *Aiki and Yamagata* [2000] on the propagation of isolated eddies are consistent with Euler's momentum integral theorem and results of numerous studies of eddy motion on a β-plane [e. g. *McWilliams and Flierl*, 1979; *Flierl*, 1984; *Killworth*, 1986; *McWilliams et al.*, 1986; *Cushman-Roisin et al.*, 1990]. The same theorem also predicts that anticyclonic eddies move westward faster than cyclonic eddies. Further, nonlinearity also induces meridional motion [*Chassignet and Cushman-Roisin*, 1991], northward for cyclonic eddies and southward for anticyclonic eddies.

[60] The studies mentioned above assume that isolated eddies move through an environment at rest. Existence of a background flow alters eddy propagation speeds in both the zonal and meridional directions [*McWilliams and Flierl*, 1979; *Chang and Philander*, 1989; *Sutyrin and Flierl*, 1994; *Holland and Mitchum*, 2001]. In the case of an eddy influenced by a westward flow (e.g., an anticyclonic eddy in the NEC in the lee of the island of Hawaii), its westward propagation is likely to be increased provided that the westward flow is not too fast and the shear in the westward flow is small, as in the example discussed by *Holland and Mitchum* [2001].

[61] When eddies are not isolated from each other, interactions among them may influence their propagation substantially. *Davey and Killworth* [1989] found a solution to show that the effect of a chain of connected anticyclonic eddies is to retard their westward propagation. Two eddies of the same sign may merge into one [*Nof and Simon*, 1987]. Two eddies of opposite signs in close proximity may result in the weaker one rotating around the stronger one, or move in parallel lines if they are of similar strength [*Kundu*, 1990].

[62] In summary, there are at least 4 factors that could potentially influence eddy propagation: strength of forcing, sign of an eddy, background flow, and eddy-eddy interaction, which poses a great challenge in predicting the movement of an eddy. In general, we may expect stronger eddies propagate faster than weaker ones, cyclonic eddies follow a northwestward path, anticyclonic eddies follow a southwestward path, and anticyclonic eddies translate westward faster than cyclonic eddies due to nonlinear eddy dynamics and the presence of the NEC. Eddy behavior as observed by satellite altimetry and in the main model experiments supports this general pattern (e.g., Figures 1a and 8).

[63] All these aspects can also be seen in the auxiliary experiment, STRONG, in which strong trade winds are applied for the entire duration of the experiment. This experiment is analogous to the idealized experiments of *Davey and Killworth* [1989] and *Aiki and Yamagata* [2000] but in a general circulation setting. At the start of the experiment, very weak cyclonic and moderate anticyclonic flows are present at sites C_0 and A_0 respectively. Within about 40 days, an anticyclonic eddy is spun up at site A_0 and shed. In the meantime, a cyclonic eddy is also spun up at site C_0 and shed 10 days after the departure of the anticyclonic eddy. During the entire integration period, a total of 12 anticyclonic eddies and 10 cyclonic eddies are generated at sites A_0 and C_0 respectively in an almost alternating manner,

but not regularly as predicted by idealized modeling studies of *Davey and Killworth* [1989] and *Aiki and Yamagata* [2000].

[64] Seven of the anticyclonic eddies with spin-up times of 30–120 days follow a southwestward path to reach the regional domain boundary within 4 months; three with shorter spin-up times (10–25 days) take large north-south swings before their signatures become unidentifiable in the domain - interactions with nearby eddies distort both the shape and path of these eddies; the last two are still in the domain at the end of the integration. Four of the cyclonic eddies with spin-up times of 50–120 days follow a northwestward path to reach the regional domain boundary within 5 months – the fastest crossing time is approximately 3 months by a strong cyclonic eddy with a spin-up time of 120 days taking the most direct route; four with shorter spin-up times (20–30 days) dissipate within 2 months, two of which travel southward initially (see discussion in the next paragraph); two remain in the domain at the end of the integration. Eddies with longer spin-up times tend to be stronger too. It is unclear why there is such a large range in the spin-up time even under constant wind-forcing. We shall consider this question in a future investigation.

[65] There have been recorded cases of cyclonic eddies moving southward instead of their expected northwestward propagation in observations. Several cyclonic eddies studied by *Patzert* [1969] and *Lumpkin* [1998] were noted to travel southward initially before changing course to the typical northwestward direction. Advection by nearby anticyclonic eddies was thought to be the cause. Cyclonic eddy Opal observed during E-Flux III exhibited such a behavior. The center of Opal moved southward from 20°N to 19°N from 11 to 21 March 2005 [*Dickey et al.*, 2008]. The altimetry shows that an anticyclonic eddy was propagating away from the island while Opal was spinning up. The southward flow associated with the anticyclonic eddy was very strong, which may have pulled Opal southward. In May–June 2008, a newly spun-up cyclonic eddy was advected by the strong southward flow of an anticyclonic eddy shed earlier (Figure 7a). The cyclonic eddy was then merged into a passing cyclonic eddy from the east south of the anticyclonic eddy. A similar propagation pattern also occurs in the QSCAT experiment in February 2008 (Figure 7b). In this case the cyclonic eddy travels southward following the rotation of the anticyclonic eddy shed earlier, and then the two eddies propagate westward together with the cyclonic eddy at a lower latitude, a case of eddy-eddy interaction at work. Since the two types of eddies are usually in close vicinity, initial southward shift of a growing cyclonic eddy often occurs.

6. Summary

[66] The ocean west of the main Hawaiian Islands is characterized by enhanced EKE due to the presence of strong mesoscale eddies frequently generated in the region. Two mechanisms of eddy generation in the lee of the island of Hawaii, oceanic flow around an oceanic barrier as hypothesized by *McGary* [1955] and *Manar* [1967] and atmospheric flow around an atmospheric barrier as proposed by *Patzert* [1969], are examined in this study using numerical model experiments. Eddy generation characteristics in the model experiments are contrasted and compared

with that in the altimetry record to determine the applicability of the two mechanisms.

[67] Eddy generation by oceanic flow in the lee of the island of Hawaii requires the presence of fast westward flows through the Alenuihaha Channel and around the South Point of the island. Model solution of the Q-MEAN experiment does show episodic westward flows at these two locations, and the generation of eddies by these flows. The resulting EKE, however, is too low to account for the observed level of regional enhancement due to the relatively weaker intensity of the eddies that also appear less frequently than in altimetry.

[68] Eddy generation by atmospheric flow in the lee of the island of Hawaii is based on the wind shear distribution caused by the prevailing northeasterly trade winds funneling through the Alenuihaha Channel and accelerating around the South Point with a wind minimum in the island lee. Oceanic upwelling and downwelling occur in regions of surface divergence (the northern part of the island lee) and convergence (the southern part of the island lee) through differential Ekman transport, and may be generically categorized as a sink and a source to the ocean interior respectively. The different regimes of circulation from the idealized modeling studies of *Davey and Killworth* [1989] and *Aiki and Yamagata* [2000] provide an explanation of eddy generation under strong and persistent trade wind conditions and the lack of it during periods of weak trade wind and no trade wind conditions in observations. The close relationship between wind and eddy generation is exhibited in the solutions of the main model experiments. Further, model solutions of the QSCAT and Q-NOHI experiments show regionally enhanced EKE that resemble well the observed pattern and intensity.

[69] The QSCAT experiment shows good agreement with altimetry in terms of eddy occurrences in the lee of the island of Hawaii because of the strong dependency of eddy generation on winds. Major discrepancies are in eddy propagation due to the complex nature of eddy-eddy interactions. Although prediction of eddy generation may be attempted by inspecting recent eddy events and wind conditions, predicting the path of an eddy poses a great challenge because eddy strength, shape and type all affect how the eddy interacts with other eddies nearby.

References

Aiki, H., and T. Yamagata (2000), Successive formation of planetary lenses in an intermediate layer, *Geophys. Astrophys. Fluid Dyn.*, *92*, 1–29, doi:10.1080/03091920008203709.

Armi, L., and W. Zenk (1984), Large lenses of highly saline Mediterranean water, *J. Phys. Oceanogr.*, *14*, 1560–1576, doi:10.1175/1520-0485 (1984)014<1560:LLOHSM>2.0.CO;2.

Barton, E. D., G. Basterretxea, P. Flament, E. G. Mitchelson-Jacob, B. Jones, J. Arístegui, and H. Felix (2000), Lee region of Gran Canaria, *J. Geophys. Res.*, *105*, 17,173–17,193, doi:10.1029/2000JC900010.

Basterretxea, G., E. D. Barton, P. Tett, P. Sangrà, E. Navarro-Perez, and J. Arístegui (2002), Eddy and DCM response to wind-shear in the lee of Gran Canaria, *Deep Sea Res., Part I*, 49, 1087–1101, doi:10.1016/S0967-0637(02)00009-2.

Batchelor, G. K. (1967), *An Introduction to Fluid Dynamics*, 515 pp., Cambridge Univ. Press, Cambridge, U. K.

Bidigare, R. R., C. Benitez-Nelson, C. L. Leonard, P. D. Quay, M. L. Parsons, D. G. Foley, and M. P. Seki (2003), Influence of a cyclonic eddy on microheterotroph biomass and carbon export in the lee of Hawaii, *Geophys. Res. Lett.*, 30(6), 1318, doi:10.1029/2002GL016393.

Blayo, E., and L. Debreu (2005), Revisiting open boundary conditions from the point of view of characteristic variables, *Ocean Modell.*, 9, 231–252, doi:10.1016/j.ocemod.2004.07.001.

Bleck, R. (2002), An oceanic general circulation model framed in hybrid isopycnic-Cartesian coordinates, *Ocean Modell.*, 4, 55–88, doi:10.1016/S1463-5003(01)00012-9.

Browning, G., and H.-O. Kreiss (1982), Initialization of the shallow water equations with open boundaries by the bounded derivative method, *Tellus*, 34, 334–351, doi:10.1111/j.2153-3490.1982.tb01823.x.

Calil, P. H. R., and K. J. Richards (2010), Transient upwelling hot spots in the oligotrophic North Pacific, *J. Geophys. Res.*, 115, C02003, doi:10.1029/2009JC005360.

Calil, P. H. R., K. J. Richards, Y. Jia, and R. R. Bidigare (2008), Eddy activity in the lee of the Hawaiian Islands, *Deep Sea Res., Part II*, 55, 1179–1194, doi:10.1016/j.dsr2.2008.01.008.

Chang, P., and S. G. H. Philander (1989), Rossby wave packets in baroclinic mean currents, *Deep Sea Res., Part I*, 36, 17–37, doi:10.1016/0198-0149(89)90016-2.

Chassignet, E. P., and B. Cushman-Roisin (1991), On the influence of a lower layer on the propagation of nonlinear oceanic eddies, *J. Phys. Oceanogr.*, 21, 939–957, doi:10.1175/1520-0485(1991)021<0939:OTIOAL>2.0.CO;2.

Chassignet, E. P., L. T. Smith, G. R. Halliwell, and R. Bleck (2003), North Atlantic simulation with the Hybrid Coordinate Ocean Model (HYCOM): Impact of the vertical coordinate choice, reference pressure, and thermobaricity, *J. Phys. Oceanogr.*, 33, 2504–2526, doi:10.1175/1520-0485(2003)033<2504:NASWTH>2.0.CO;2.

Chassignet, E. P., et al. (2006), Generalized vertical coordinates for eddy-resolving global and coastal ocean forecast, *Oceanography*, 19(1), 118–129.

Chassignet, E. P., et al. (2009), US GODAE: Global ocean prediction with the Hybrid Coordinate Ocean Model (HYCOM), *Oceanography*, 22(2), 64–75, doi:10.5670/oceanog.2009.39.

Chavanne, C., P. Flament, R. Lumpkin, B. Dousset, and A. Bentamy (2002), Scatterometer observations of wind variations induced by oceanic islands: Implications for wind-driven ocean circulation, *Can. J. Remote Sens.*, 28, 466–474, doi:10.5589/m02-047.

Chavanne, C., P. Flament, and K.-W. Gurgel (2010), Interactions between a submesoscale anticyclonic vortex and a front, *J. Phys. Oceanogr.*, 40, 1802–1818, doi:10.1175/2010JPO4055.1.

Cummings, J. A. (2005), Operational multivariate ocean data assimilation, *Q. J. R. Meteorol. Soc.*, 131, 3583–3604, doi:10.1256/qj.05.105.

Cushman-Roisin, B., E. P. Chassignet, and B. Tang (1990), Westward motion of isolated eddies, *J. Phys. Oceanogr.*, 20, 758–768, doi:10.1175/1520-0485(1990)020<0758:WMOME>2.0.CO;2.

Davey, M. K., and P. D. Killworth (1989), Flows produced by discrete sources of buoyancy, *J. Phys. Oceanogr.*, 19, 1279–1290, doi:10.1175/1520-0485(1989)019<1279:FPBDSO>2.0.CO;2.

Dickey, T. D., F. Nencioli, V. S. Kuwahara, C. Leonard, W. Black, Y. M. Rii, R. R. Bidigare, and Q. Zhang (2008), Physical and bio-optical observations of oceanic cyclones west of the island of Hawaii, *Deep Sea Res., Part II*, 55, 1195–1217, doi:10.1016/j.dsr2.2008.01.006.

Dong, C., J. C. McWilliams, and A. F. Shchepetkin (2007), Island wakes in deep water, *J. Phys. Oceanogr.*, 37, 962–981, doi:10.1175/JPO3047.1.

Dong, C., T. Mavor, F. Nencioli, S. Jiang, Y. Uchiyama, J. C. McWilliams, T. Dickey, M. Ondrusek, H. Zhang, and D. K. Clark (2009), An oceanic cyclonic eddy on the lee side of Lanai Island, Hawaii, *J. Geophys. Res.*, 114, C10008, doi:10.1029/2009JC005346.

Firing, E. (1996), Currents observed north of Oahu during the first five years of HOT, *Deep Sea Res., Part II*, 43, 281–303, doi:10.1016/0967-0645(95)00097-6.

Flierl, G. R. (1984), Rossby wave radiation from a strongly nonlinear warm eddy, *J. Phys. Oceanogr.*, 14, 47–58, doi:10.1175/1520-0485(1984)014<0047:RWRFAS>2.0.CO;2.

Halliwell, G. R. (2004), Evaluation of vertical coordinate and vertical mixing algorithms in the Hybrid Coordinate Ocean Model (HYCOM), *Ocean Modell.*, 7, 285–322, doi:10.1016/j.ocemod.2003.10.002.

Holland, C. L., and G. T. Mitchum (2001), Propagation of Big Island eddies, *J. Geophys. Res.*, 106, 935–944, doi:10.1029/2000JC000231.

Jia, Y. (2000), Formation of an Azores current due to Mediterranean overflow in a modeling study of the North Atlantic, *J. Phys. Oceanogr.*, 30, 2342–2358, doi:10.1175/1520-0485(2000)030<2342:FOAACD>2.0.CO;2.

Jiménez, B., P. Sangrà, and E. Mason (2008), A numerical study of the relative importance of wind and topographic forcing on oceanic eddy shedding by tall, deep water islands, *Ocean Modell.*, 22, 146–157, doi:10.1016/j.ocemod.2008.02.004.

Kara, A. B., A. J. Wallcraft, C. N. Barron, H. E. Hurlburt, and M. A. Bourassa (2008), Accuracy of 10 m winds from satellites and NWP products near land-sea boundaries, *J. Geophys. Res.*, 113, C10020, doi:10.1029/2007JC004516.

Kersalé, M., A. M. Doglioli, and A. A. Petrenko (2011), Sensitivity study of the generation of mesoscale eddies in a numerical model of Hawaii Islands, *Ocean Sci.*, 7, 277–291, doi:10.5194/os-7-277-2011.

Killworth, P. D. (1986), On the propagation of isolated multilayer and continuously stratified eddies, *J. Phys. Oceanogr.*, 16, 709–716, doi:10.1175/1520-0485(1986)016<0709:OTPOIM>2.0.CO;2.

Kobashi, F., and H. Kawamura (2001), Variation of sea surface height at periods of 65–220 days in the subtropical gyre of the North Pacific, *J. Geophys. Res.*, 106, 26,817–26,831, doi:10.1029/2000JC000361.

Kundu, P. K. (1990), *Fluid Mechanics*, 638 pp., Academic, San Diego, Calif.

Kuwahara, V. S., F. Nencioli, T. D. Dickey, Y. M. Rii, and R. R. Bidigare (2008), Physical dynamics and biological implications of Cyclone Noah in the lee of Hawaii during E-Flux I, *Deep Sea Res., Part II*, 55, 1231–1251, doi:10.1016/j.dsr2.2008.01.007.

Large, W. G., and S. Pond (1981), Open ocean momentum flux measurements in moderate to strong winds, *J. Phys. Oceanogr.*, 11, 324–336, doi:10.1175/1520-0485(1981)011<0324:OOMFMI>2.0.CO;2.

Lumpkin, C. F. (1998), Eddies and currents of the Hawaiian Islands, Ph.D. thesis, 282 pp., Sch. of Ocean and Earth Sci. and Technol., Univ. of Hawaii at Mānoa, Honolulu.

Luyten, J. R., and H. M. Stommel (1986), Experiments with cross-gyre flow patterns on a beta-plane, *Deep Sea Res., Part A*, 33, 963–972, doi:10.1016/0198-0149(86)90009-9.

Manar, T. A. (1967), Progress in 1965–66 at the Bureau of Commercial Fisheries Biological Laboratory, Honolulu, *USFWS Circ. 274*, 51 pp., U.S. Fish and Wildlife Serv., Washington, D. C.

McGary, J. W. (1955), Mid-Pacific oceanography, Part VI, Hawaiian offshore waters, December 1949–November 1951, *Spec. Sci. Rep.* 152, 138 pp., U.S. Fish and Wildlife Serv., Washington, D. C.

McWilliams, J. C., and G. R. Flierl (1979), On the evolution of isolated, nonlinear vortices, *J. Phys. Oceanogr.*, 9, 1155–1182, doi:10.1175/1520-0485(1979)009<1155:OTEOIN>2.0.CO;2.

McWilliams, J. C., P. R. Gent, and N. J. Norton (1986), The evolution of balanced, low-mode vortices on the β-plane, *J. Phys. Oceanogr.*, 16, 838–855, doi:10.1175/1520-0485(1986)016<0838:TEOBLM>2.0.CO;2.

Nencioli, F., V. S. Kuwahara, T. D. Dickey, Y. M. Rii, and R. R. Bidigare (2008), Physical dynamics and biological implications of a mesoscale eddy in the lee of Hawaii: Cyclone Opal observations during E-Flux III, *Deep Sea Res., Part II*, 55, 1252–1274, doi:10.1016/j.dsr2.2008.02.003.

Niiler, P. P., N. A. Maximenko, and J. C. McWilliams (2003), Dynamically balanced absolute sea level of the global ocean derived from near-surface velocity observations, *Geophys. Res. Lett.*, 30(22), 2164, doi:10.1029/2003GL018628.

Nof, D., and L. M. Simon (1987), Laboratory experiments on the merging of nonlinear anticyclonic eddies, *J. Phys. Oceanogr.*, 17, 343–357, doi:10.1175/1520-0485(1987)017<0343:LEOTMO>2.0.CO;2.

Patzert, W. (1969), Eddies in Hawaiian waters, *Tech. Rep. HIG-69-8*, Hawaii Inst. of Geophys., Univ. of Hawaii at Mānoa, Honolulu.

Pedlosky, J. (1983), Eastern boundary ventilation and the structure of the thermocline, *J. Phys. Oceanogr.*, 13, 2038–2044, doi:10.1175/1520-0485(1983)013<2038:EBVATS>2.0.CO;2.

Pedlosky, J. (1996), *Ocean Circulation Theory*, 453 pp., Springer, Berlin.

Piedeleu, M., P. Sangrà, A. Sánchez-Vidal, J. Fabrés, and C. Gordo (2009), An observational study of oceanic eddy generation mechanisms by tall deep-water islands (Gran Canaria), *Geophys. Res. Lett.*, 36, L14605, doi:10.1029/2008GL037010.

Pullen, J., J. D. Doyle, P. May, C. Chavanne, and P. Flament (2008), Monsoon surges trigger oceanic eddy formation and propagation in the lee of the Philippine Islands, *Geophys. Res. Lett.*, 35, L07604, doi:10.1029/2007GL033109.

Qiu, B., D. A. Koh, C. Lumpkin, and P. Flament (1997), Existence and formation mechanism of the North Hawaiian Ridge Current, *J. Phys. Oceanogr.*, 27, 431–444, doi:10.1175/1520-0485(1997)027<0431:EAFMOT>2.0.CO;2.

Sangrà, P., M. Auladell, A. Marrero-Díaz, J. L. Pelegrí, E. Fraile-Nuez, Á. Rodríguez-Santana, J. M. Martín, E. Mason, and A. Hernández-Guerra

(2007), On the nature of oceanic eddies shed by the island of Gran Canaria, *Deep Sea Res., Part I*, *54*, 687–709, doi:10.1016/j.dsr. 2007.02.004.

Sangrà, P. A., et al. (2009), The Canary eddy corridor: A major pathway for long-lived eddies in the subtropical North Atlantic, *Deep Sea Res., Part I*, *56*, 2100–2114, doi:10.1016/j.dsr.2009.08.008.

Seki, M. P., J. J. Polovina, R. E. Brainard, R. R. Bidigare, C. L. Leonard, and D. G. Foley (2001), Biological enhancement at cyclonic eddies tracked with GOES thermal imagery in Hawaiian waters, *Geophys. Res. Lett.*, *28*, 1583–1586, doi:10.1029/2000GL012439.

Smith, R. B., and V. Grubisic (1993), Aerial observations of Hawaii's wake, *J. Atmos. Sci.*, *50*, 3728–3750, doi:10.1175/1520-0469(1993) 050<3728:AOOHW>2.0.CO;2.

Stommel, H. (1982), Is the South Pacific helium plume dynamically active?, *Earth Planet. Sci. Lett.*, *61*, 63–67, doi:10.1016/0012-821X (82)90038-3.

Stommel, H., A. B. Arons, and A. J. Faller (1958), Some examples of stationary planetary flow patterns in bounded basins, *Tellus*, *10*, 179–187, doi:10.1111/j.2153-3490.1958.tb02003.x.

Sutyrin, G. G., and G. R. Flierl (1994), Intense vortex motion on the beta plane: Development of the beta gyres, *J. Atmos. Sci.*, *51*, 773–790, doi:10.1175/1520-0469(1994)051<0773:IVMOTB>2.0.CO;2.

van Dyke, M. (1982), *An Album of Fluid Motions*, 174 pp., Parabolic, Stanford, Calif.

von Kármán, T. (1954), *Aerodynamics: Selected Topics in Light of Their Historical Development*, Cornell Univ. Press, Ithaca, N. Y.

Xie, S.-P., W. T. Liu, Q. Liu, and M. Nonaka (2001), Far-reaching effects of the Hawaiian Islands on the Pacific ocean-atmosphere system, *Science*, *292*, 2057–2060, doi:10.1126/science.1059781.

Yu, Z., N. Maximenko, S.-P. Xie, and M. Nonaka (2003), On the termination of the Hawaiian Lee Countercurrent, *Geophys. Res. Lett.*, *30*(5), 1215, doi:10.1029/2002GL016710.

P. H. R. Calil, National Institute of Water and Atmospheric Research, Private Bag 14901, 301 Evans Bay Parade, Wellington 6021, New Zealand.

E. P. Chassignet, Center for Ocean-Atmosphere Prediction Studies, Florida State University, 200 R. M. Johnson Bldg., Tallahassee, FL 32306, USA.

Y. Jia, J. T. Potemra, and K. J. Richards, International Pacific Research Center, School of Ocean and Earth Science and Technology, University of Hawai'i at Mānoa, 1680 East West Rd., POST Bldg. 401, Honolulu, HI 96822, USA. (yjia@hawaii.edu)

E. J. Metzger and A. J. Wallcraft, Ocean Dynamics and Prediction Branch, Naval Research Laboratory, Code 7323, Stennis Space Center, MS 39529, USA.